



Kent Academic Repository

Galloway, Johanna M., Senior, Laura, Fletcher, Jordan M., Beesley, Joseph L., Hodgson, Lorna R., Harniman, Robert L., Mantell, Judith M., Coombs, Jennifer, Rhys, Guto G., Xue, Wei-Feng and others (2018) *Bioinspired Silicification Reveals Structural Detail in Self-Assembled Peptide Cages*. ACS Nano, 12 (2). pp. 1420-1432. ISSN 1936-0851.

Downloaded from

<https://kar.kent.ac.uk/65831/> The University of Kent's Academic Repository KAR

The version of record is available from

<https://doi.org/10.1021/acsnano.7b07785>

This document version

Author's Accepted Manuscript

DOI for this version

Licence for this version

UNSPECIFIED

Additional information

Versions of research works

Versions of Record

If this version is the version of record, it is the same as the published version available on the publisher's web site. Cite as the published version.

Author Accepted Manuscripts

If this document is identified as the Author Accepted Manuscript it is the version after peer review but before type setting, copy editing or publisher branding. Cite as Surname, Initial. (Year) 'Title of article'. To be published in *Title of Journal*, Volume and issue numbers [peer-reviewed accepted version]. Available at: DOI or URL (Accessed: date).

Enquiries

If you have questions about this document contact ResearchSupport@kent.ac.uk. Please include the URL of the record in KAR. If you believe that your, or a third party's rights have been compromised through this document please see our [Take Down policy](https://www.kent.ac.uk/guides/kar-the-kent-academic-repository#policies) (available from <https://www.kent.ac.uk/guides/kar-the-kent-academic-repository#policies>).

Kent Academic Repository

Full text document (pdf)

Citation for published version

Galloway, Johanna M and Senior, Laura and Fletcher, Jordan M and Beesley, Joseph L and Hodgson, Lorna R and Harniman, Robert L and Mantell, Judith M and Coombs, Jennifer and Rhys, Guto G and Xue, Wei-Feng and Mosayebi, Majid and Linden, Noah and Liverpool, Tanniemola B and Curnow, Paul and Verkade, Paul and Woolfson, Derek N (2018) Bioinspired Silicification

DOI

<https://doi.org/10.1021/acsnano.7b07785>

Link to record in KAR

<http://kar.kent.ac.uk/65831/>

Document Version

Author's Accepted Manuscript

Copyright & reuse

Content in the Kent Academic Repository is made available for research purposes. Unless otherwise stated all content is protected by copyright and in the absence of an open licence (eg Creative Commons), permissions for further reuse of content should be sought from the publisher, author or other copyright holder.

Versions of research

The version in the Kent Academic Repository may differ from the final published version.

Users are advised to check <http://kar.kent.ac.uk> for the status of the paper. **Users should always cite the published version of record.**

Enquiries

For any further enquiries regarding the licence status of this document, please contact:

researchsupport@kent.ac.uk

If you believe this document infringes copyright then please contact the KAR admin team with the take-down information provided at <http://kar.kent.ac.uk/contact.html>

1
2
3
4
5
6
7
8
9
10
11
12
13
14
15
16
17
18
19
20
21
22
23
24
25
26
27
28
29
30
31
32
33
34
35
36
37
38
39
40
41
42
43
44
45
46
47
48
49
50
51
52
53
54
55
56
57
58
59
60

Bioinspired Silicification Reveals Structural Detail in Self-assembled Peptide Cages

Johanna M. Galloway,^{†,} Laura Senior,[‡] Jordan M. Fletcher,[†] Joseph L. Beesley,^{†,‡} Lorna R. Hodgson,[‡] Robert L. Harniman,[†] Judith M. Mantell,^{‡,§} Jennifer Coombs,^{‡,¥} Guto G. Rhys,[†] Weifeng Xue,[⊥] Majid Mosayebi,^{||,#} Noah Linden,[#] Tanniemola B. Liverpool,^{||,#} Paul Curnow,^{‡,||} Paul Verkade,^{‡,§,||} and Derek N. Woolfson^{†,‡,||*}*

[†] School of Chemistry, University of Bristol, Cantock's Close, Bristol, BS8 1TS, UK.

[‡] School of Biochemistry, University of Bristol, Biomedical Sciences Building, University Walk, Bristol, BS8 1TD, UK.

[§] Wolfson Bioimaging Facility, University of Bristol, Biomedical Sciences Building, University Walk, Bristol, BS8 1TD, UK.

[¥] Bristol Centre for Functional Nanomaterials, NSQI, Tyndall Avenue, University of Bristol, Bristol, BS8 1FD, UK.

[⊥] School of Biosciences, Stacy Building, University of Kent, Canterbury, CT2 7NJ, UK.

^{||} BrisSynBio, University of Bristol, Life Sciences Building, Tyndall Avenue, Bristol, BS8 1TQ, UK.

1
2
3 # School of Mathematics, University Walk, University of Bristol, Bristol BS8 1TW, United
4
5
6 Kingdom.

7
8
9 **Corresponding authors**

10
11 *E-mail: d.n.woolfson@bristol.ac.uk

12
13 ORCID iD DNW: 0000-0002-0394-3202

14
15
16
17 *E-mail: johanna.galloway@bristol.ac.uk

18
19 ORCID iD JMG: 0000-0003-3998-0870

20
21
22
23
24
25
26 **Keywords**

27
28 atomic force microscopy, bioinspired nanoparticles, biomineralization, coiled-coil peptides,
29
30 electron microscopy, peptide design

31
32
33
34
35
36
37 **Abstract**

38
39
40
41 **Understanding how molecules in self-assembled soft-matter nanostructures are organized**
42 **is essential for improving the design of next-generation nanomaterials. Imaging these**
43 **assemblies can be challenging and usually requires processing, *e.g.* staining or embedding,**
44 **which can damage or obscure features. An alternative is to use bioinspired mineralization,**
45 **mimicking how certain organisms use biomolecules to template mineral formation.**
46
47
48
49
50
51 **Previously, we have reported the design and characterization of Self-Assembled peptide**
52 **caGEs (SAGEs) formed from *de novo* peptide building blocks. In SAGEs, two**
53 **complementary, three-fold symmetric, peptide hubs combine to form a hexagonal lattice,**
54
55
56
57
58
59
60

1
2
3 which curves and closes to form SAGE nanoparticles. As hexagons alone cannot tile onto
4 spheres, the network must also incorporate non-hexagonal shapes. While the hexagonal
5 ultrastructure of the SAGEs has been imaged, these defects have not been observed. Here,
6 we show that positively charged SAGEs biotemplate a thin, protective silica coating.
7 Electron microscopy shows that these SiO₂-SAGEs do not collapse, but maintain their 3D
8 shape when dried. Atomic force microscopy reveals a network of hexagonal and irregular
9 features on the SiO₂-SAGE surface. The dimensions of these (7.2 nm ± 1.4 nm across,
10 internal angles 119.8° ± 26.1°) accord with the designed SAGE network and with coarse-
11 grained modelling of SAGE assembly. The SiO₂-SAGEs are permeable to small molecules
12 (<2 nm), but not to larger biomolecules (>6 nm). Thus, bioinspired silicification offers a
13 mild technique that preserves soft-matter nanoparticles for imaging, revealing structural
14 details <10 nm in size, whilst also maintaining desirable properties, such as permeability to
15 small molecules.
16
17
18
19
20
21
22
23
24
25
26
27
28
29
30
31
32
33
34
35
36
37

38 In nature, organisms construct soft-matter nanostructures to define and stabilize the form and
39 function of the cell. Natural self-assembled functional soft-matter architectures include: coat
40 proteins that protect viral genetic cargo and facilitate cell penetration for replication; protein and
41 lipid structures that are used to compartmentalize, manufacture and transport materials in
42 bacterial and mammalian cells; and combinations of carbohydrate-based materials and lipid-
43 protein membranes that define bacterial and plant cell walls. Biomolecular engineers take
44 inspiration from these natural systems to design nanostructured materials that assemble from the
45 bottom up. The self-assembling building blocks used can be based on natural, engineered or
46 completely *de novo* biomolecules, including: peptides,^{1,2} proteins,^{3,4} lipids,⁵ polymers,⁶ and
47
48
49
50
51
52
53
54
55
56
57
58
59
60

1
2
3 DNA.⁷ In turn, these materials have been adapted for use in a wide range of medical and
4
5 biotechnological applications.^{3,5,7}
6
7

8 Imaging the organization of bioinspired self-assembled materials at the molecular or nanoscale
9
10 is essential for both confirming the targeted designs, and for advancing understanding of how to
11
12 assemble and apply these materials in the future. However, imaging nanoscale biomolecular
13
14 structures is challenging, as they are small, flexible, typically not very electron dense, and
15
16 assembled *via* weak non-covalent interactions. Staining, embedding, coating, or crosslinking can
17
18 all help to tackle these challenges and aid the visualization of soft structures.⁸ Nonetheless, such
19
20 processing can also introduce unwelcome artifacts, or disrupt these delicate architectures.⁸ Thus
21
22 simple, non-destructive processing methods that provide contrast are still required. Here we take
23
24 inspiration from nature, and demonstrate the use of bioinspired mineralization to preserve the 3D
25
26 structure of soft, peptide-based, self-assembled nanoparticles.
27
28
29
30

31 In biomineralization biomolecules direct the precipitation of minerals to produce hierarchical
32
33 composite tissues.^{9,10} Over 60 biominerals occur in natural biological systems,¹¹ including:
34
35 calcium carbonate,¹² calcium phosphate,^{13,14} magnetite,¹⁵ and silica.^{16–19} For example, diatoms
36
37 are unicellular eukaryotic algae that construct intricate silicified cell walls, called frustules, using
38
39 biomolecules such as long-chain polyamines,²⁰ and proteins such as arginine- and lysine-rich
40
41 silaffins,^{21,22} cingulins,²³ and phosphorylated silicidins.²⁴ These biomolecules are thought to
42
43 direct silica to precipitate from soluble silicic acid *in vivo*.^{21,22} Silicification has been studied *in*
44
45 *vitro* using positively charged bio-inspired molecules, such as lysine-rich polypeptides^{22,25} and
46
47 other polyamines.²⁶ The size of the biotemplated silica structures usually correlates with their
48
49 pre-silicified size in solution.²⁷ As such, silica coating has been used to preserve soft-matter
50
51 nanostructures faithfully.^{27–31} In pioneering work from the Brinker Lab, this has been extended to
52
53
54
55
56
57
58
59
60

1
2
3 coat cells^{32,33} and even whole organisms.³⁴ This allowed features to be clearly imaged in 3D
4
5 down to ≈ 10 nm.³¹ Permeable biomineral coatings have also been used to protect soft-matter
6
7 structures for use in medicine^{35,36} and catalysis.^{37,38} In these ways, bioinspired silicification is
8
9 able to provide contrast for nanoscale imaging and stabilize the function of soft-matter structures.
10
11

12
13 Protein cages are specifically addressable soft-matter nanostructures with potential biomedical
14
15 applications in drug targeting and delivery,^{39–42} vaccination,^{4,43} and in biotechnology as
16
17 nanoreactors.^{44–46} An example of these is the Self-Assembled peptide caGEs (SAGEs, Figure 1).¹
18
19 The SAGEs are rationally designed¹ from fully characterized *de novo* peptide components.⁴⁷
20
21 Specifically, a parallel α -helical coiled-coil peptide homotrimer, CC-Tri3, is linked *via* a
22
23 disulfide bond and back-to-back to one of two obligate heterodimers, CC-Di-A or CC-Di-B,¹
24
25 making two complementary hubs (hub A and hub B) each with 3-fold symmetry. When these
26
27 hubs are mixed, the heterodimers are formed, and these drive the self-assembly of what is
28
29 intended to be a hexagonal network. Surprisingly, when imaged by electron microscopy (EM)
30
31 and using in-liquid atomic force microscopy (AFM) closed, spherical particles are observed. This
32
33 is rationalized by *in silico* molecular-dynamics simulations of small patches of the SAGE
34
35 network, which consistently indicate that these multi-peptide structures curve in one direction.¹
36
37 However, hexagons alone cannot tile on a sphere and are unable to form closed, convex, regular
38
39 Platonic solids.⁴⁸ C₆₀ (Buckminsterfullerene)⁴⁹ combines 20 hexagons with 12 pentagons to form
40
41 a closed Archimedean solid structure.⁴⁸ Thus, the SAGE network must incorporate irregularities
42
43 to form spherical nanoparticles. It is not known if these consist of holes in the lattice, or if non-
44
45 hexagonal or irregular polygons close the structures. To date, such features on the SAGE surface
46
47 have not been observed. Therefore, we sought a method that could reveal how the peptides are
48
49 organized in SAGE particles.
50
51
52
53
54
55
56
57
58
59
60

1
2
3 Here we describe the application of bioinspired silicification to form a stabilizing permeable
4 coating on the SAGEs. We show that this allows detailed imaging of their surfaces. AFM of the
5 silica-coated SAGEs (SiO₂-SAGEs) reveals a hexagonal network as designed. Moreover, with
6 ≈ 7 nm vertex-to-vertex lengths, the size of these polygons is fully consistent with the designed
7 underlying peptide network. The network predominantly comprises regular hexagons, but other
8 shapes, which are required to form a closed object from a hexagonal lattice, are also apparent.
9 This concurs with coarse-grained computational modelling that we have recently performed.⁵⁰
10 As the silicified SAGEs can be imaged clearly using standard EM and AFM techniques,
11 bioinspired silicification offers a facile technique for preserving soft-matter nanostructures in 3D
12 so that their self-organization can be studied. In addition, silicification offers a route to
13 stabilizing soft, self-assembled materials for use in bionanotechnology and synthetic
14 biology.^{35,36,51}
15
16
17
18
19
20
21
22
23
24
25
26
27
28
29
30
31
32
33
34

35 **Results and Discussion**

36 **The *N* and *C* termini of the SAGE Homotrimer can be Decorated with Positive Charge**

37
38 Molecular dynamics (MD) simulations of a hexagonal peptide network designed for the
39 ‘parent’ SAGE indicate that the arrays curve.¹ In the MD, the long axes of the trimeric coiled-
40 coil units remain perpendicular to the plane of the array, whereas the dimeric components rotate
41 freely about the two disulfide bonds. Moreover, the direction of curvature is consistent across the
42 simulations, with the *N* termini of the homotrimers presented on the convex (*i.e.* external) face of
43 the SAGEs, while the *C* termini are on the concave interior. This is our working model for
44 SAGE structure and it provides a basis for further design.
45
46
47
48
49
50
51
52
53
54
55
56
57
58
59
60

For this study, tetra-arginine (R4) or tetra-lysine (K4) peptides were appended to either the *N* or *C* terminus of the homotrimer (CC-Tri3, Figure 1, Table 1 & S1 – S3). The aim being that, when assembled into SAGEs, these constructs would present positively charged residues on the external or internal surfaces of SAGEs for *N*-terminal or *C*-terminal appendages, respectively. In turn, these should act as templates to localize and precipitate silica from aqueous silicic acid onto the peptide cages. In this way, we aimed to create SiO₂-SAGE particles. As controls, negatively charged tetra-glutamate (E4) variants were also generated, which should be poor at biotemplating silica.²⁵

Table 1. Summary of the main peptide sequences used to assemble decorated SAGEs for silicification. Systematic names of the trimer components used to make the hubs, their amino-acid sequences, and their overall charge as calculated using pepcalc.⁵² See supplementary information for further details of the naming system (Table S1), mixing peptide hubs to form SAGEs (Table S2), and the full amino-acid sequences for all peptides used in this study (Table S3).

trimer name	sequence	net charge at pH 7
CC-Tri3	Ac-GEIAAIKKEIAAIKCEIAAIKQGYG-Am	0.9
E4-CC-Tri3	Ac-EEEEGGGEIAAIKKEIAAIKCEIAAIKQGYG-Am	-3.1
CC-Tri3-E4	Ac-GEIAAIKKEIAAIKCEIAAIKQGYGGGEEEE-Am	-3.1
K4-CC-Tri3	Ac-KKKKGGGEIAAIKKEIAAIKCEIAAIKQGYG-Am	4.9
CC-Tri3-K4	Ac-GEIAAIKKEIAAIKCEIAAIKQGYGGGKKKK-Am	4.9
R4-CC-Tri3	Ac-RRRRGGGEIAAIKKEIAAIKCEIAAIKQGYG-Am	4.9
CC-Tri3-R4	Ac-GEIAAIKKEIAAIKCEIAAIKQGYGGRRRR-Am	4.9

Peptides were synthesized, purified and assembled into SAGE peptide hubs (Figure S1, Table 1 & S1 – S4 for sequences, naming and characterization). For the *C*-terminally decorated trimers,

1
2
3
4
5
6
7
8
9
10
11
12
13
14
15
16
17
18
19
20
21
22
23
24
25
26
27
28
29
30
31
32
33
34
35
36
37
38
39
40
41
42
43
44
45
46
47
48
49
50
51
52
53
54
55
56
57
58
59
60

CC-Tri3-K4 and CC-Tri3-R4, circular dichroism (CD) spectra gave α helicities similar to the undecorated parent homotrimer (CC-Tri3), and as predicted based on the peptide sequences (Figure S2 & S3 and Table S5). Moreover, these three constructs had very similar thermal unfolding transitions, with midpoints (T_M s) of 54 °C, 57 °C, and 56 °C, respectively (Figure S2 and Table S5). By contrast, appending positive charge to the *N* termini reduced the α helicities and also the T_M values to 33 °C and 34 °C for the K4 and R4 variants, respectively (Figure S2 & S3, and Table S5). CC-Tri3 variants with negatively charged E4 blocks at the *N* and *C* termini showed the opposite behavior: the former was as folded and stable as the parent ($T_M = 65.5$ °C), whereas the latter was as destabilized ($T_M = 31$ °C) as the *N*-terminal K4 and R4 variants, Figure S2 & S3, and Table S5. These changes in stability of CC-Tri3 when charge is appended mirror a recent study of free-standing α -helical peptides.⁵³ They can be explained in terms of repulsive interactions between the blocks and the partial charges associated with the helical backbone, which are positive and negative for the *N* and *C* termini, respectively.⁵³ Analytical ultracentrifugation (AUC) sedimentation velocity (SV) and sedimentation equilibrium (SE) experiments conducted at room temperature with the parent and decorated homotrimers returned molecular weights consistent with trimeric coiled-coil assemblies for each construct in solution, Figure S4, Table S6.

Together, these data for the modified CC-Tri3 peptides show that they are stably folded and trimeric at room temperature, albeit with some of the thermal stabilities compromised. Therefore, we continued with these variants, using them to construct decorated hubs for the assembly of modified SAGE particles.

Positive Charge Localizes Silica Biomineralization onto SAGEs

1
2
3 Herein, we refer to the unmodified parent assemblies as SAGE, Figure 2a, and the SAGE
4 variants as follows: E4-SAGE, K4-SAGE and R4-SAGE for the *N*-terminally decorated
5 particles, Figure 2e; and SAGE-E4, SAGE-K4 and SAGE-R4 for the *C*-terminally decorated
6 structures, Figure 2i. Acidification of sodium silicate forms a mixture of metastable ortho- and
7 oligosilicic acids.⁵⁴ For simplicity, we refer to this as ‘silicic acid’. Polymerization of these
8 mixtures were monitored by fluorescence of 2-(4-pyridyl)-5-((4-(2-
9 dimethylaminoethylaminocarbonyl)methoxy)phenyl)oxazole (PDMPO) without and with the
10 various SAGE particles (Figure S5). The PDMPO indicated that the different SAGEs did not
11 appear to alter the amount or rate of bulk silica precipitation. The silicification of SAGEs to form
12 discrete biomineralized particles was optimized to form electron dense particles (Figure 2 & S6).
13
14
15
16
17
18
19
20
21
22
23
24
25
26

27 As controls, silicification of the peptide hubs alone—*i.e.*, negatively charged hub A, or
28 positively charged hub B—formed mesh networks with poor contrast, Figure S7; and similar
29 precipitates were observed with short positively charged peptides, GYGKKKK and GYGRRRR,
30 Figure S8. By comparison, with both hub A and hub B present—*i.e.*, with SAGEs formed—
31 silica particles were observed, and these were particularly clear with excellent contrast for the
32 K4- and R4-decorated SAGEs, Figures 2, S6 & S7.
33
34
35
36
37
38
39
40

41 In more detail, the *C*-terminal tetra-arginine decoration, SAGE-R4, gave large, slightly
42 interconnected, and polydispersed spheres (305 nm ± 120 nm). The tetra-lysine variants,
43 K4-SAGE and SAGE-K4, assembled into an interconnected mesh and smaller, slightly
44 interconnected spheres (Figure 2g & k and S6e & h). The most monodisperse and unconnected
45 nanospheres were formed by *N*-terminal tetra-arginine decorated R4-SAGEs, Figure 2h & S6f.
46
47
48
49
50
51
52
53
54
55
56
57
58
59
60
These were 213 nm ± 84 nm in diameter, Table S7, Figure 2h, S6h & S9. This is a significant
increase in size and decrease of the distribution compared with unmineralized R4-SAGEs

1
2
3 (109 nm \pm 84 nm), which were difficult to measure as they gave poor contrast (Figure S10).
4
5 Similarly, the silicified R4-SAGEs gave better quality scanning electron microscope (SEM)
6
7 images, revealing clearer particles when compared to unmineralized R4-SAGEs (Figure S11).
8
9 Energy dispersive X-ray (EDX) spectra confirmed the presence of silicon (Si K α = 1.74 keV)
10
11 and oxygen (O K α = 0.53 keV) in the SiO₂-R4-SAGEs (Figure S12). The absence of any
12
13 coherent electron diffraction patterns, however, indicated that the silica coatings are likely
14
15 amorphous rather than a crystalline polymorph of silica.
16
17
18

19
20 In summary to this section, a combination of TEM, SEM and EDX demonstrates that SAGEs
21
22 can be modified with cationic tetra-peptides to generate discrete, spherical, silicified
23
24 nanoparticles, which we refer to as SiO₂-SAGEs. The best of these preparations were made from
25
26 R4-SAGEs, which we used next to optimize conditions for preparing SiO₂-SAGEs.
27
28
29

30 **The Formation of Discrete SiO₂-SAGEs can be Optimized**

31
32 R4-SAGEs were mineralized with a range of silicic acid concentrations (0 mM – 36 mM),
33
34 imaged (Figure S13), and grainsized (Table S7). Without silicic acid, or at low concentrations
35
36 (6 mM), it was difficult to discern structures by TEM, and the grains were polydisperse. At
37
38 36 mM silicic acid, large interconnected SiO₂-R4-SAGE particles were clear (217 nm \pm 58 nm).
39
40 We propose that high silicic acid concentrations deposit a thicker layer of SiO₂, leading to
41
42 particle aggregation. Optimal mineralization occurred at 12 mM – 24 mM silicic acid, leading to
43
44 discrete SiO₂-R4-SAGE spheres with sizes distributed around \approx 200 nm in diameter (Figure 2h).
45
46
47

48
49 Next, we varied the peptide concentration between 2 μ M – 25 μ M peptide for K4 and R4
50
51 SAGE variants, and mineralized these with 24 mM silicic acid at 20 °C (Figure S14). At low
52
53 peptide concentrations (2 μ M – 5 μ M), the K4- and R4-SAGE constructs formed discrete
54
55 mineralized spheres similar to those noted above. At the higher peptide concentrations (10 μ M –
56
57
58
59
60

1
2
3 25 μM), much larger micron-sized mesh and network structures were observed, which is
4
5 consistent with our observations that unmineralized SAGEs aggregate at high μM
6
7 concentrations.
8
9

10 The SAGE system is modular, which means that the hub modules can be mixed and matched
11 to tune the SAGE properties. Thus far, both hub A and hub B carried the E4, K4 or R4
12 decorations, *i.e.* they were 100% decorated. To vary this, first we prepared SAGEs with
13 undecorated parent hub A plus hub B fully decorated with K4 or R4 (Figure S15). These were
14 silicified using standard conditions of 2 μM peptide, 24 mM silicic acid, 10 mM phosphate (PI)
15 buffer pH 7.4, 20 $^{\circ}\text{C}$, 24 hours. Compared with 100% decoration, these 50% decorated SAGEs
16 form smaller particles, particularly for the R4 variants. R4-SAGEs displaying between 50%-
17 100% tetra-arginine were prepared by combining R4-hub B and mixtures of hub A with and
18 without the R4 decoration (Figure S16). The less highly charged SAGEs, *i.e.* 50% - 80%
19 R4-SAGE, formed smaller interconnected mineralized silica particles, with average diameters of
20 60 nm – 90 nm, Table S8; whereas the 90% and 100% R4-SAGEs formed the larger but
21 nonetheless discrete structures noted above.
22
23
24
25
26
27
28
29
30
31
32
33
34
35
36
37

38 100% R4-SAGEs were also assembled and silicified at a range of temperatures (4 $^{\circ}\text{C}$ – 37 $^{\circ}\text{C}$).
39 This range should not significantly perturb the silicification process,⁵⁵ but, as the midpoint
40 unfolding temperature (T_{M}) of CC-R4-Tri3 is 34 $^{\circ}\text{C}$, this range could affect homotrimer folding,
41 and thus SAGE assembly (Figure S17). At 4 $^{\circ}\text{C}$, the mineralized particles were small (77 nm
42 \pm 26 nm) interconnected spheres. At 20 $^{\circ}\text{C}$, the particles were larger (213 nm \pm 84 nm) and
43 discrete, and were larger still (330 nm \pm 168 nm) and clumped together at 25 $^{\circ}\text{C}$. At 37 $^{\circ}\text{C}$,
44 smaller (105 nm \pm 42 nm) interconnected spheres were formed. Thus, the optimal temperature
45 for assembling discrete mineralized R4-SAGEs is at \approx 20 $^{\circ}\text{C}$, where the CC-R4-Tri3 should be
46
47
48
49
50
51
52
53
54
55
56
57
58
59
60

1
2
3 well folded, but there is enough thermal energy to avoid forming the small, interconnected
4
5 structures assembled at lower temperatures.
6
7

8 Finally, the components for 100% R4-SAGEs were mixed at between pH 5.5 – 8.0, and the
9
10 products silicified at the assembly pH. At low pH, silica formation is known to be slowed, but
11
12 the 24-hour mineralization used should be ample for silica formation.⁵⁵ TEM images (Figure
13
14 S18) reveal that silicification at neutral pH (7.0 and 7.4) led to discrete spherical particles;
15
16 whereas at higher pH values (7.5 – 8.0), interconnected SAGEs resembling those formed at
17
18 higher (36 mM) silicic acid concentrations were formed, which we attribute to rapid and more
19
20 complete precipitation of silica. At slightly lower pH values (6.5 and 6.0) spheres were
21
22 discernible, but these were embedded in meshes. Finally, at pH 5.5 only thin sheets are visible,
23
24 which we ascribe to the precipitation of silica by largely unfolded aggregated peptide.
25
26
27
28

29 Thus, we find that for R4-SAGE particles, which provide the best substrates for silicification,
30
31 there are optimal conditions for mineralization to produce SiO₂-R4-SAGEs. These are
32
33 summarized in Figure 3, and comprise: 2 – 5 μM peptide, 90 – 100% R4-decorated hubs, 20 °C,
34
35 pH 7.0 – 7.4 PI buffer, mineralized with 12 – 24 mM silicic acid for 24 hours.
36
37
38

39 **The 3D Structure of SiO₂-SAGEs can be Visualized by EM Tomography and AFM**

40
41 We recorded TEM tilt series for SiO₂-R4-SAGEs and used these to construct tomograms and
42
43 3D models of the mineralized particles (Movie S1 – S4, Figure S19). The tomograms show that
44
45 the particles did not collapse significantly when dried onto TEM grids; *i.e.*, dried
46
47 SiO₂-R4-SAGEs retained their 3D structure. SiO₂-R4-SAGEs were also imaged by tapping-
48
49 mode atomic force microscopy (TM-AFM) and PeakForce AFM (PF-AFM), Figure S20. AFM
50
51 measurements of unmineralized SAGEs show significant collapse of the peptide particles upon
52
53 drying to an aspect ratio (AR) between the height z and the diameter in x and y of ≈ 0.1 .¹ By
54
55
56
57
58
59
60

1
2
3 contrast, the dried SiO₂-R4-SAGEs had an aspect ratio of ≈ 0.7 in AFM. Thus, the silica coating
4
5 reinforces SiO₂-R4-SAGEs against collapse.
6
7

8 We were interested to see if silicification also preserved the structure of the peptide building
9
10 blocks and pores between the hub subunits anticipated from the original design, Figure S21.
11 PF-AFM was used to map variations in the height, adhesion and dissipation properties of the
12
13 surface of a cluster of SiO₂-R4-SAGEs (Figure 4). Despite variations in the topography due to
14
15 the near-spherical shape of the SiO₂-R4-SAGEs, the surfaces of the nanoparticles could be
16
17 imaged. This revealed a polygonal lattice texture on the surface of all the SiO₂-R4-SAGEs
18
19 imaged (Figure S22).
20
21
22
23

24 Interrogation of these patterns on individual SiO₂-R4-SAGEs with PF-AFM identified
25
26 polygons with vertex-to-vertex spacings of $7.2 \text{ nm} \pm 1.4 \text{ nm}$ (Figure 5). This is entirely
27
28 consistent with the SAGE design.¹ Moreover, these features were apparent in the height,
29
30 adhesion and dissipation plots, with regions of increased height and adhesion co-localized,
31
32 Figure 5e, h & i. The network was also seen in phase contrast in TM-AFM (Figure S23f & i).
33
34 Ridges, created by the peptide framework within the biotemplated silica, should present as raised
35
36 lattice structures on the curved SAGE surface with increased height, nanoscale roughness and
37
38 flexibility when compared to a silica-filled pore (Figure S21). This was indeed observed in
39
40 PF-AFM, with raised ridges corresponding to higher adhesion (roughness) and dissipation
41
42 (flexibility) when compared to the pore centers, and confirmed by positive phase shifts on ridges
43
44 in TM-AFM.
45
46
47
48
49

50 Interestingly, the AFM data also revealed variations in the originally intended hexagonal
51
52 network (Figure 5j & l). To help quantify the extent of these variations, a model for a smooth
53
54 non-symmetric convex surface was fitted to the height data to flatten the dome shape of the
55
56
57
58
59
60

1
2
3
4
5
6
7
8
9
10
11
12
13
14
particle (Figure S24b). This generated a topology map of the particle, highlighting variance due to surface features (*i.e.* pores and ridges). The internal angles of the polygonal structures from unflattened images were distributed around 120° ($119.4^\circ \pm 26.9^\circ$, Figure S24d). Nonetheless, other angles—*e.g.* for pentagons (108.0°), heptagons (128.6°) and irregular polygons—also fell comfortably within the distribution.

15
16
17
18
19
20
21
22
23
24
25
26
27
28
29
30
31
32
33
34
35
36
37
38
39
40
41
42
43
44
45
46
47
The internal angles measured from coarse-grained modelling of SAGE assembly (see Mosayebi *et al.*⁵⁰ and Figure S24c & d) showed a major peak centered on hexagonal polygons ($122.0^\circ \pm 25.0^\circ$), which agrees well with the experimental data. However, there was also a small peak for squares at $89.6^\circ \pm 8.6^\circ$, which is not observed experimentally. The squares are likely to be due to the simulated network, which comprises obligate heteromeric pairings of pure hubs (*i.e.*, hub A and hub-B only), not being able to access odd-sided polygons, *e.g.* pentagons, to close the SAGEs. In the experimental system, however, non-hexagonal polygons could form by non-cognate peptide interactions (*i.e.*, CC-Di-B to CC-Di-B, or CC-Di-A to CC-Di-A), especially as hubs of same type are brought into close proximity during assembly. Alternatively, as the peptide hubs are inherently dynamic, the homotrimers may exchange to form mixed hubs, which would also increase the chances of incorporating non-hexagonal structures. The current simulations do not allow for subunit exchange in hubs, and penalize homomerization of the heterodimer components, both of which would facilitate the formation of the odd-sided polygons by SAGE hubs during assembly. This will be corrected in future coarse-grained models.

48
49
50
51
52
53
54
55
56
57
58
59
60
These observations indicate how the peptide lattice adapts to close, and leads us to refine our initial hypothesis for SAGE assembly and structure, which centered on the formation and propagation of hexagonal peptide arrays, Figure 1.¹ The inclusion of non-hexagonal and irregular shapes, as revealed herein using the SiO₂-SAGE system and supported by coarse-grained

1
2
3 computational modelling of SAGE assembly (*vide infra*),⁵⁰ presents a clear mechanism for
4 closure. The variations that we see are not evenly spaced on the surface (Figure 5f – m, S24) as
5 required in Archimedean solids,⁴⁸ so the SAGE peptides self-assemble to form more complex,
6 irregular polyhedra.
7
8
9
10

11 **SiO₂-SAGEs are Permeable to Small Molecules and Peptides, but not to Proteins**

12
13 Permeable biomineral coatings have been used to protect enzymes,^{37,38} drug cargos,⁵⁶ and
14 vaccines.^{35,36,51} With a view to using SiO₂-SAGEs in these contexts, we tested their permeability
15 to small molecules and proteins. To do this, we set up a reporter system, which uses the
16 modularity of SAGE system to introduce a fluorophore into the peptide fabric of the SAGEs,
17 Figure 6a. A R4-SAGE preparation was doped with 2.5% of hub B harboring carboxyfluorescein
18 (hub B-fl). When silicified, these R4-SAGE-fls formed particles indistinguishable from
19 R4-SAGEs by TEM, Figure 6b. Moreover, the particles were fluorescent, and correlative light
20 and electron microscopy (CLEM)^{57,58} showed that this fluorescence co-localized with the
21 particles observed by TEM, Figure 6c & d, and S25. Consistent with this, prior to silicification
22 R4-SAGE-fls were difficult to visualize by TEM, but fluorescent particles were clear by light
23 microscopy (LM), Figure S26. We found that higher concentrations of silicic acid (36 mM)
24 reduced detection of the fluorescence signal, and, therefore, used intermediate silicic acid
25 concentrations (12 – 24 mM) to form thinner silica coatings.
26
27
28
29
30
31
32
33
34
35
36
37
38
39
40
41
42
43
44
45

46 To monitor small-molecule ingress into SiO₂-R4-SAGE-fls, we used the fluorescence
47 quencher Trypan blue, which must contact the fluorophore to quench it.^{59,60} Trypan blue is small
48 ($\approx 1.5 \times 0.5 \times 0.5$ nm), and was able to quench the fluorescence of both R4-SAGE-fls and
49 SiO₂-R4-SAGE-fls, Figure 6f, j & n. The SAGE structures were still visible in bright-field LM
50
51
52
53
54
55
56
57
58
59
60

1
2
3 images (Figure S26), indicating that Trypan blue can traverse the silica coating to effect
4
5 quenching.
6
7

8 For delivery applications, small-molecule cargos must be able to exit the host vehicle. Tris(2-
9 carboxyethyl)phosphine hydrochloride (TCEP) reduces the disulfide bonds used to construct the
10 SAGE hubs, and so disassembles SAGE particles.¹ TCEP treatment reduced the number and
11 intensity of fluorescent SiO₂-R4-SAGE-fls particles, Figure 6g, k & o, consistent with disruption
12 of SAGEs and the release of peptides from the biomineralized structures (CC-Tri3 is ≈3.0 x 1.5 x
13 1.5 nm when folded). Nonetheless, particles were still visible by bright-field LM and TEM after
14 this treatment, Figure S26 – S27, demonstrating that the biomineral replicas remain intact after
15 TCEP treatment to remove the peptides.
16
17
18
19
20
21
22
23
24
25
26

27 Finally, to test if larger proteins penetrated the silica barrier, R4-SAGE-fls and
28 SiO₂-R4-SAGE-fls were treated with the protease trypsin. For the former, non-mineralized
29 particles fluorescent puncta were lost, Figure 6h, indicating proteolysis of the SAGE peptides
30 and release of the fluorophores. However, with the SiO₂-R4-SAGE-fls these objects remained
31 visible indicating that the silica coat protected the peptides from proteolysis by trypsin, Figure 6l
32 & p. The trypsin may be too large (≈7.0 x 6.0 x 5.5 nm) to penetrate the silicified SAGEs, or
33 may adhere to the silica coat because it has a pI of ≈10. However, as the pI of CC-Tri3 (≈9) and
34 trypsin are similar and the smaller CC-Tri3-fl does appear to traverse the silica coating, it is
35 unlikely that charge alone is responsible for preventing proteolysis of the SiO₂-SAGEs by
36 trypsin. Together, these data indicate that SiO₂-SAGEs are permeable to small molecules (<2 nm
37 across), including fluorescence quenchers, reducing agents and the peptide building blocks of the
38 SAGEs themselves, but not to larger (≈6 nm across) protein molecules such as trypsin.
39
40
41
42
43
44
45
46
47
48
49
50
51
52
53
54
55
56
57
58
59
60

Conclusions and Future Directions

Herein we demonstrate that SAGE particles can be decorated with positive charge, assembled and controllably silicified under mild conditions in aqueous buffer. We find that an *N*-terminal tetra-arginine tag—to give R4-SAGEs—forms discrete silica-coated particles. We have tuned the particle size between $\approx 50 - 200$ nm by controlling the proportion of tetra-arginine in the SAGE particles; and by optimizing silicic acid concentration, and also the conditions for SAGE assembly (peptide concentration, temperature and pH). We envisage this ability to control particle size and functionalization could allow silicified SAGE particles to be tailored for use in a range of biotechnological applications. We find that SiO₂-SAGEs particles do not form below pH 6.0, and that they aggregate above pH 7.5. This suggests that SAGE particles assembled at or near neutral pH could then be disassembled under acidic conditions. Such pH-triggered disassembly could be used to release encapsulated cargos controllably within target cells, as acidification during endosomal trafficking should lead to disassembly and thus delivery.⁶¹

SiO₂-SAGEs maintain their 3D structure when dried, which facilitates imaging of the underlying polygonal peptide network. The network shows predominantly hexagonal shapes ≈ 7 nm across, consistent with our original design and *in silico* models.^{1,50} However, and interestingly, it also reveals the presence of non-hexagonal and irregular polygons with internal angles distributed evenly about the hexagonal 120°. These are necessary to close the network, as hexagons alone cannot tile on a sphere. These experimental measurements largely concur with a coarse-grained computational model for SAGE assembly that we are developing,⁵⁰ which shows the dominance of a hexagonal arrangement of hubs, and highlights the importance of non-hexagonal polygons to achieve closure. However, the simulations suggest that square arrangements of hubs should be more abundant than we observe experimentally. This current

1
2
3 model disfavors mechanisms that can access odd-sided polygons in the lattice, *e.g.* homotypic
4 association of the two heterodimer components or exchange within the homotrimer core to form
5 mixed hubs. The AFM data show that peptide network within SiO₂-R4-SAGEs is able to form
6 internal angles consistent with odd-sided polygons rather than closing using squares. In turn, this
7 indicates that defects formation *via* one of the above two or other mechanisms must be in
8 operation during SAGE assembly. These new concepts and the experimental data from the
9 SiO₂-SAGEs are being incorporated into a revised coarse-grained model to explore the formation
10 of odd- and even-sided hub assemblies.
11
12
13
14
15
16
17
18
19
20
21

22 As the SAGEs are closed by small shape defects rather than by large holes in the lattice, any
23 larger cargos contained within SAGEs should not leak out. This bodes well for using them to
24 support active proteins and enzymes;^{45,46} for drug encapsulation, targeting and delivery;^{42,62} and
25 as antigen presentation vaccine platforms.^{3,4} Biomineral coatings are currently used to protect
26 drug cargos,^{56,63} vaccines^{36,51} and enzymes^{37,64} by stabilizing biomolecules against thermal and
27 other degradation. Thus, bioinspired silicification of SAGEs functionalized for use in medical or
28 biotechnological applications could afford similar protection to these particles. SAGEs could
29 also be designed to template other materials.^{65,66} For example, SAGEs displaying antigens could
30 be coated with adjuvantive⁵¹ and/or protective³⁶ calcium phosphate to create stabilized vaccine
31 formulations with improved efficacies and shelf-lives. SAGEs displaying ligands for cell-surface
32 receptors and disease treatment could also be decorated with gold nanoparticles to combine
33 targeting, imaging and treatment of diseased cells;⁶⁷ or SAGEs coated with platinum
34 nanoparticles could evolve hydrogen more effectively than disordered Pt nanoparticles.⁶⁸ The
35 SAGE system has clear attributes to facilitate such applications, including its modularity, our
36 ability to redesign it, and the ease with which the SAGE components can be functionalized.
37
38
39
40
41
42
43
44
45
46
47
48
49
50
51
52
53
54
55
56
57
58
59
60

1
2
3 Therefore, by mixing and matching appropriately modified hub components, there is
4 considerable potential to develop a range of tailored multifunctional organic, inorganic, and/or
5
6
7
8 biologically decorated SAGEs for future applications.
9

10 11 12 13 14 **Materials and Methods**

15
16 For extended materials and methods, see the Supporting Information.

17
18 Peptides were synthesized using Fmoc solid-phase synthesis⁶⁹ on Rink amide resin in a
19 LibertyTM microwave peptide synthesizer on 0.1 mM scales (see Tables S1 – S3). Each amino
20 acid was coupled (5 eq. of Fmoc amino acid, 4.5 eq. of hydroxybenzotriazole (HOBt), 10 eq. of
21 *N,N'*-diisopropylcarbodiimide (DIC) in 7 mL dimethylformamide (DMF) with 25 W microwave
22 irradiation at 50 °C for 5 minutes), washed (5 x 7 mL DMF), deprotected (20% (v/v) morpholine
23 in DMF, with 20 W microwave irradiation at 75 °C for 5 minutes), and then washed before the
24 next amino acid was added. Assembled peptides were acetylated on resin (3 eq. acetic anhydride,
25 4.5 eq. of *N,N*-diisopropylethylamine (DIPEA) in 7 mL DMF for 30 minutes). Peptides were
26 cleaved from the resin with 94% (v/v) trifluoroacetic acid (TFA), 2% (v/v) 1,2-ethanedithiol
27 (EDT), 2% (v/v) water and 2% (v/v) triisopropylsilane (TIPS) for 3 hours. Peptides were filtered,
28 precipitated using diethyl ether (Et₂O), pelleted (4000 xg, 10 minutes, 4 °C), and freeze dried.
29
30
31
32
33
34
35
36
37
38
39
40
41
42
43
44

45 Peptides were purified using reverse phase high pressure liquid chromatography (RP-HPLC)
46 on a Kromatek (semi-micro, 5 μm, 100 Å, 10 mm ID x 150 mm L) C18 column, using a linear
47 gradient of buffer A (0.1% (v/v) TFA in water) and 20% - 80% buffer B (0.1% (v/v) TFA in
48 MeCN). Purified peptide peaks were analyzed by matrix-assisted laser desorption / ionization –
49 time of flight mass spectrometry (MALDI-TOF) and analytical RP-HPLC. For 2,2'-
50 dipyrityldisulfide (DPDS) thiol activation⁷⁰ of heterodimer A or B, ≈5 mg of heterodimer was
51
52
53
54
55
56
57
58
59
60

1
2
3 dissolved in 5 mL of water or phosphate buffered saline (PBS, 137 mM NaCl, 2.7 mM KCl,
4 10 mM phosphate buffer, pH 7.4). 10 eq. DPDS in 1 mL methanol (MeOH) was added. After
5
6 1 hour, excess DPDS was removed using 3 x 30 mL Et₂O, and the activated peptide freeze dried,
7
8 purified using RP-HPLC, characterized (MALDI-TOF and analytical RP-HPLC), and freeze
9
10 dried. To form hubs, each homotrimer was mixed with an activated heterodimer in equimolar
11
12 amounts in PBS ($\approx 1 \text{ mg mL}^{-1}$ peptide), and mixed for 3 hours at 20 °C. Hubs were purified by
13
14 RP-HPLC, and characterized (MALDI-TOF and analytical RP-HPLC, Figure S1 & Table S4).
15
16
17
18
19

20 Circular dichroism (CD) spectra were recorded at between 5 °C – 90 °C using a JASCO J-810
21
22 spectropolarimeter fitted with a Peltier temperature controller. A 1 mm path length quartz cuvette
23
24 containing 50 μM peptide in phosphate buffer (PI, 10 mM potassium phosphate (8.02 mM
25
26 dibasic K_2HPO_4 , 1.98 mM monobasic KH_2PO_4) pH 7.4) and 250 μM tris(2-
27
28 carboxyethyl)phosphine hydrochloride (TCEP) was heated at 40 °C hour^{-1} . The Mean Residue
29
30 Ellipticity (MRE) at 222 nm was recorded every 1 °C, and full CD spectra (190 nm – 260 nm)
31
32 were recorded every 5 °C. Analytical ultracentrifugation (AUC) was performed on each
33
34 homotrimer (325 μM peptide in PI, 1.625 mM TCEP and 25 mM NaCl). Sedimentation velocity
35
36 (SV) and sedimentation equilibrium (SE) experiments were conducted using Beckman Optima
37
38 XL-A and XL-I analytical ultracentrifuges with An-60 and An-50 rotors, respectively, and at
39
40 20 °C. For SV, samples were spun at 60 krpm with 120 scans collected between 5.8 cm – 7.3 cm
41
42 and data fitted using SEDFIT.⁷¹ For SE, data were collected at 6 rotor speeds between 30 krpm –
43
44 48 krpm, and fitted with a single ideal species model using Ultrascan II.⁷² The partial specific
45
46 volumes (\bar{v}) for each peptide, buffer densities and viscosities were calculated using
47
48 SEDNTERP⁷³ (Table S6).
49
50
51
52
53
54
55
56
57
58
59
60

1
2
3 Typically for silicification, SAGEs were assembled (2 μM hub A + 2 μM hub B) in PI buffer
4
5 for 1 hour at 20 $^{\circ}\text{C}$, then 500 μL of these samples were mixed with 500 μL PI buffer containing
6
7 0 mM – 36 mM freshly prepared silicic acid,⁷⁴ and washed 3x with water after 24 hours. 0.5 μL
8
9 2-(4-pyridyl)-5-((4-(2-dimethylaminoethylaminocarbamoyl)methoxy)phenyl)oxazole (PDMPO,
10
11 LysoTracker®)⁷⁵ was added to 100 μL of mineralization solution to monitor the polymerization
12
13 of silica in solution by fluorescence emission.
14
15

16
17 For scanning electron microscopy (SEM), samples were dried on silicon wafers fixed to an
18
19 aluminum stub. Unmineralized samples were coated with ≈ 5 nm Au-Pd using an Emtech 575X
20
21 sputter coater. Stubs were imaged in a FEI Quanta FEG-SEM. Samples were dried on carbon
22
23 coated copper grids and imaged on a Tecnai 12 – FEI 120 kV BioTwin Spirit transmission
24
25 electron microscope (TEM). Tilt series between angles of $\approx 70^{\circ}$ and $\approx -70^{\circ}$ for tomographic
26
27 reconstructions were collected using a Tecnai 20 – FEI 200 kV Twin Lens Scanning
28
29 Transmission Electron Microscope (STEM). Images were collected using an FEI Eagle 4k x 4k
30
31 CCD camera. Grainsizes of SiO_2 -SAGEs were measured from representative TEM images using
32
33 ImageJ,^{76,77} and distributions fitted in Origin 2015 64 bit (Equation S3). Tilt series were aligned
34
35 and reconstructed using eTomo in the IMOD^{78,79} software package (University of Colorado,
36
37 Boulder). 3D reconstructions of tomograms were rendered in Amira 3D (FEI Software). Movie
38
39 files of the tomographic reconstruction software outputs were compiled in ImageJ⁷⁶ and
40
41 compressed using HandBrake. Energy dispersive X-ray (EDX) spectra were recorded using a
42
43 JEOL 2100F STEM and a Gatan Orius 11 megapixel 832 camera. X-rays were detected using an
44
45 80 mm^2 AZtec detector, and processed using AZtecTEM software. For correlative light and
46
47 electron microscopy (CLEM),^{57,58} fluorescent R4-SAGE-fls were imaged first using a Leica
48
49
50
51
52
53
54
55
56
57
58
59
60

1
2
3 DMI4000 B inverted epifluorescence microscope, then using a TEM (see above). Fluorescence
4 was overlain with TEM images using the TurboReg plug-in in Fiji.⁸⁰
5
6
7

8 Tapping Mode Atomic Force Microscopy (TM-AFM) was performed on a Multi-mode
9 microscope with a Quadrexed Nanoscope III controller using Scout-Beta cantilevers (NuNano,
10 Bristol, UK). PeakForce AFM (PF-AFM) was conducted on a Multi-mode VIII microscope with
11 Nanoscope V controller and a fast scan head unit in combination with SCANASYST-AIR-HR
12 cantilevers (Bruker, CA, USA). Data was analyzed using Nanoscope Analysis 1.5 software
13 (Bruker, CA, USA) and scripts written in Matlab (Mathworks). Design and parameterization of
14 the coarse-grained computational modelling is described in Mosayabi *et al.*⁵⁰
15
16
17
18
19
20
21
22
23

24 The permeability of particles to small molecules was tested using silica-coated and unsilicified
25 fluorescent R4-SAGE-fls. 1 mL of washed silicified SAGE was pelleted (17,000 xg, 5 minutes,
26 20 °C) and resuspended in 100 μ L PI buffer, and 10 μ L added to 30 μ L PI buffer. As a control,
27 40 μ L of unmineralized fluorescent SAGE was used. Samples were made up to a total volume of
28 50 μ L by PI buffer (control, no additive), or PI buffer plus a fluorescence quenching molecule
29 (10 μ L 0.4% (w/v) Trypan blue, 2 hours at 20 °C), a reducing agent (10 μ L 5 mM tris(2-
30 carboxyethyl)phosphine hydrochloride (TCEP), 2 hours at 20 °C), or a protease (trypsin, 5 μ L
31 1 mg mL⁻¹, 2 hours at 37 °C). Samples were transferred to slides and imaged on a fluorescence
32 microscope (detailed above).
33
34
35
36
37
38
39
40
41
42
43
44
45
46
47
48

49 **Associated Content**

50
51 The authors declare no competing financial interests.
52
53
54

55 The following files in support of this manuscript are available free of charge on the ACS
56 Publications website (<http://pubs.acs.org/>) at DOI XXXX:
57
58
59
60

1
2
3 SiO₂-SAGE_SI.pdf contains: Extended methods, supplementary notes, figures and tables that
4
5 include: analytical RP-HPLC, MALDI-TOF, AUC data, CD data, PDMPO fluorescence spectra,
6
7 TEM images, grainsizing, SEM images, AFM plots, CLEM images, bright-field and
8
9 fluorescence LM images, and diagrams.
10

11
12
13 Tomograms and reconstruction movies: tilt series 29,000x magnification - S1 29kx tomo.avi; and
14
15 at 50,000x magnification - S2 50kx tomo.avi. 3D reconstructions of the 50,000 x magnification
16
17 series rotating equatorially - S3 50kx 3D1.avi, and polar - S4 50kx 3D2.avi.
18
19
20
21
22
23

24 **Author Contributions**

25
26
27 JMG, JMF, PC and DNW conceived the project, designed the experiments and drafted the
28
29 manuscript. JMG and LS performed the mineralization experiments, and JMG recorded TEM
30
31 and SEM images and reconstructed tomograms with JMM, JC and LRH. JMG performed
32
33 grainsizing. JMG and JLB synthesized the peptides, conducted the solution-phase biophysics and
34
35 fluorescence microscopy. JMG, JLB and LRH recorded fluorescence and TEM images for
36
37 CLEM with PV and JC. JMG and RLH recorded the AFM data and analyzed them with W-FX.
38
39 JMG and GGR recorded and analyzed the AUC data. MM, NL and TBL performed the coarse-
40
41 grained computational modelling. The manuscript was written through contributions of all
42
43 authors. All authors have given approval to the final version of the manuscript.
44
45
46
47
48
49
50
51

52 **Funding Sources**

53
54
55 JMG, LRH, JMM, W-FX, PV & DNW are supported by the BBSRC (BB/M002969/1). PC and
56
57 LS are supported by the European Research Council (282101). DNW holds a Royal Society
58
59
60

1
2
3 Wolfson Research Merit Award (WM140008). PC, PV, TBL, MM and DNW are members of
4
5 BrisSynBio, a BBSRC/EPSRC funded Synthetic Biology Research Centre (BB/L01386X/1).
6
7
8 PF-AFM was carried out in the Chemical Imaging Facility, University of Bristol with equipment
9
10 funded by the EPSRC (EP/K035746/1). Mass spectra were recorded using the EPSRC-funded
11
12 equipment (EP/K03927X/1) School of Chemistry Mass Spectrometry Facility, University of
13
14
15 Bristol.

20 21 **Acknowledgements**

22
23 The authors would like to thank at the University of Bristol: Jon A. Jones for recording EDX
24
25 spectra and the associated TEM images, Sarah Ratcliffe for determining the concentration of the
26
27 sodium silicate stock using ICP-AES, and James Ross for help with PyMOL images.
28
29
30
31
32
33

34 35 **References**

- 36
37 (1) Fletcher, J. M.; Harniman, R. L.; Barnes, F. R. H.; Boyle, A. L.; Collins, A.; Mantell, J.;
38
39 Sharp, T. H.; Antognozzi, M.; Booth, P. J.; Linden, N.; *et al.* Self-Assembling Cages from
40
41 Coiled-Coil Peptide Modules. *Science* **2013**, *340*, 595–599.
42
43
44
45 (2) Pandya, M. J.; Spooner, G. M.; Sunde, M.; Thorpe, J. R.; Rodger, A.; Woolfson, D. N.
46
47 Sticky-End Assembly of a Designed Peptide Fiber Provides Insight into Protein
48
49 Fibrillogenesis. *Biochemistry* **2000**, *39*, 8728–8734.
50
51
52
53 (3) Wen, A. M.; Steinmetz, N. F. Design of Virus-Based Nanomaterials for Medicine,
54
55 Biotechnology, and Energy. *Chem. Soc. Rev.* **2016**, *45*, 4074–4126.
56
57
58
59
60

- 1
2
3 (4) Schwarz, B.; Douglas, T. Development of Virus-like Particles for Diagnostic and
4 Prophylactic Biomedical Applications. *Wiley Interdiscip. Rev. Nanomed. Nanobiotechnol.*
5 **2015**, *7*, 722–735.
6
7
8
9
10
11 (5) Loh, D.; Ross, A. H.; Hale, A. H.; Baltimore, D.; Eisen, H. N. Synthetic Phospholipid
12 Vesicles Containing a Purified Viral Antigen and Cell Membrane Proteins Stimulate the
13 Development of Cytotoxic T Lymphocytes. *J. Exp. Med.* **1979**, *150*, 1067–1074.
14
15
16
17
18
19 (6) Ahmad, Z.; Shah, A.; Siddiq, M.; Kraatz, H.-B. Polymeric Micelles as Drug Delivery
20 Vehicles. *RSC Adv.* **2014**, *4*, 17028–17038.
21
22
23
24
25 (7) Veneziano, R.; Ratanalert, S.; Zhang, K.; Zhang, F.; Yan, H.; Chiu, W.; Bathe, M.
26 Designer Nanoscale DNA Assemblies Programmed from the Top down. *Science* **2016**,
27 *352*, 1534.
28
29
30
31
32
33 (8) *Methods in Cell Biology. Vol. 88: Introduction to Electron Microscopy for Biologists*;
34 Allen, T. D., Ed.; 1st ed.; Elsevier: Burlington, MA, USA, 2008.
35
36
37
38
39 (9) Mann, S. *Biomineralization: Principals and Concepts in Bioinorganic Materials*
40 *Chemistry*; Oxford University Press: Oxford, UK, 2001.
41
42
43
44 (10) Rao, A.; Cölfen, H. On the Biophysical Regulation of Mineral Growth: Standing out from
45 the Crowd. *J. Struct. Biol.* **2016**, *196*, 232–243.
46
47
48
49 (11) Metzler, R. A.; Kim, I. W.; Delak, K.; Evans, J. S.; Zhou, D.; Beniash, E.; Wilt, F.;
50 Abrecht, M.; Chiou, J.-W.; Guo, J.; *et al.* Probing the Organic-Mineral Interface at the
51 Molecular Level in Model Biominerals. *Langmuir* **2008**, *24*, 2680–2687.
52
53
54
55
56
57 (12) Meldrum, F. C.; Cölfen, H. Controlling Mineral Morphologies and Structures in
58
59
60

- 1
2
3 Biological and Synthetic Systems. *Chem. Rev.* **2008**, *108*, 4332–4432.
4
5
6
7 (13) He, G.; Dahl, T.; Veis, A.; George, A. Nucleation of Apatite Crystals in Vitro by Self-
8 Assembled Dentin Matrix Protein 1. *Nat. Mater.* **2003**, *2*, 552–558.
9
10
11
12 (14) Reid, D. G.; Duer, M. J.; Murray, R. C.; Wise, E. R. The Organic-Mineral Interface in
13 Teeth Is like That in Bone and Dominated by Polysaccharides: Universal Mediators of
14 Normal Calcium Phosphate Biomineralization in Vertebrates? *Chem. Mater.* **2008**, *20*,
15 3549–3550.
16
17
18
19
20
21
22 (15) Raschdorf, O.; Forstner, Y.; Kolinko, I.; Uebe, R.; Plitzko, J. M.; Schüler, D. Genetic and
23 Ultrastructural Analysis Reveals the Key Players and Initial Steps of Bacterial
24 Magnetosome Membrane Biogenesis. *PLoS Genet.* **2016**, *12*, Article No. e1006101.
25
26
27
28
29
30 (16) Hildebrand, M. Diatoms, Biomineralization Processes, and Genomics. *Chem. Rev.* **2008**,
31 *108*, 4855–4874.
32
33
34
35
36 (17) Jeffryes, C.; Agathos, S. N.; Rorrer, G. Biogenic Nanomaterials from Photosynthetic
37 Microorganisms. *Curr. Opin. Biotechnol.* **2015**, *33*, 23–31.
38
39
40
41 (18) Patwardhan, S. V. Biomimetic and Bioinspired Silica: Recent Developments and
42 Applications. *Chem. Commun.* **2011**, *47*, 7567–7582.
43
44
45
46
47 (19) Kharlampieva, E.; Tsukruk, T.; Slocik, J. M.; Ko, H.; Poulsen, N.; Naik, R. R.; Kröger,
48 N.; Tsukruk, V. V. Bioenabled Surface-Mediated Growth of Titania Nanoparticles. *Adv.*
49 *Mater.* **2008**, *20*, 3274–3279.
50
51
52
53
54
55 (20) Kröger, N.; Deutzmann, R.; Bergsdorf, C.; Sumper, M. Species-Specific Polyamines from
56 Diatoms Control Silica Morphology. *Proc. Natl. Acad. Sci.* **2000**, *97*, 14133–14138.
57
58
59
60

- 1
2
3
4
5
6
7
8
9
10
11
12
13
14
15
16
17
18
19
20
21
22
23
24
25
26
27
28
29
30
31
32
33
34
35
36
37
38
39
40
41
42
43
44
45
46
47
48
49
50
51
52
53
54
55
56
57
58
59
60
- (21) Kröger, N.; Lorenz, S.; Brunner, E.; Sumper, M. Self-Assembly of Highly Phosphorylated Silaffins and Their Function in Biosilica Morphogenesis. *Science* **2002**, *298*, 584–586.
- (22) Kröger, N.; Deutzmann, R.; Sumper, M. Polycationic Peptides from Diatom Biosilica That Direct Silica Nanosphere Formation. *Science* **1999**, *286*, 1129–1132.
- (23) Scheffel, A.; Poulsen, N.; Shian, S.; Kroger, N. Nanopatterned Protein Microrings from a Diatom That Direct Silica Morphogenesis. *Proc. Natl. Acad. Sci.* **2011**, *108*, 3175–3180.
- (24) Richthammer, P.; Börmel, M.; Brunner, E.; van Pée, K.-H. Biomineralization in Diatoms: The Role of Silacidins. *ChemBioChem* **2011**, *12*, 1362–1366.
- (25) Cha, J. N.; Stucky, G. D.; Morse, D. E.; Deming, T. J. Biomimetic Synthesis of Ordered Silica Structures Mediated by Block Copolypeptides. *Nature* **2000**, *403*, 289–292.
- (26) Belton, D. J.; Patwardhan, S. V.; Annenkov, V. V.; Danilovtseva, E. N.; Perry, C. C. From Biosilicification to Tailored Materials: Optimizing Hydrophobic Domains and Resistance to Protonation of Polyamines. *Proc. Natl. Acad. Sci.* **2008**, *105*, 5963–5968.
- (27) Patwardhan, S. V.; Clarson, S. J. Silicification and Biosilicification. Part 4. Effect of Template Size on the Formation of Silica. *J. Inorg. Organomet. Polym.* **2002**, *12*, 109–116.
- (28) Niu, L.; Jiao, K.; Qi, Y.; Yiu, C. K. Y.; Ryou, H.; Arola, D. D.; Chen, J.; Breschi, L.; Pashley, D. H.; Tay, F. R. Infiltration of Silica inside Fibrillar Collagen. *Angew. Chemie Int. Ed.* **2011**, *50*, 11688–11691.
- (29) Holmström, S. C.; King, P. J. S.; Ryadnov, M. G.; Butler, M. F.; Mann, S.; Woolfson, D. N. Templating Silica Nanostructures on Rationally Designed Self-Assembled Peptide

- 1
2
3
4
5
6
7
8
9
10
11
12
13
14
15
16
17
18
19
20
21
22
23
24
25
26
27
28
29
30
31
32
33
34
35
36
37
38
39
40
41
42
43
44
45
46
47
48
49
50
51
52
53
54
55
56
57
58
59
60
- Fibers. *Langmuir* **2008**, *24*, 11778–11783.
- (30) Liu, B.; Cao, Y.; Huang, Z.; Duan, Y.; Che, S. Silica Biomineralization via the Self-Assembly of Helical Biomolecules. *Adv. Mater.* **2015**, *27*, 479–497.
- (31) Qiao, Y.; Polzer, F.; Kirmse, H.; Kirstein, S.; Rabe, J. P. Nanohybrids from Nanotubular J-Aggregates and Transparent Silica Nanoshells. *Chem. Commun.* **2015**, *51*, 11980–11982.
- (32) Kaehr, B.; Townson, J. L.; Kalinich, R. M.; Awad, Y. H.; Swartzentruber, B. S.; Dunphy, D. R.; Brinker, C. J. Cellular Complexity Captured in Durable Silica Biocomposites. *Proc. Natl. Acad. Sci.* **2012**, *109*, 17336–17341.
- (33) Lou, Y.-R.; Kanninen, L.; Kaehr, B.; Townson, J. L.; Niklander, J.; Harjumäki, R.; Brinker, C. J.; Yliperttula, M. Silica Bioreplication Preserves Three-Dimensional Spheroid Structures of Human Pluripotent Stem Cells and HepG2 Cells. *Sci. Rep.* **2015**, *5*, Article No. 13635.
- (34) Townson, J. L.; Lin, Y.-S.; Chou, S. S.; Awad, Y. H.; Coker, E. N.; Brinker, C. J.; Kaehr, B. Synthetic Fossilization of Soft Biological Tissues and Their Shape-Preserving Transformation into Silica or Electron-Conductive Replicas. *Nat. Commun.* **2014**, *5*, Article No. 5665.
- (35) Wang, G.; Wang, H.-J.; Zhou, H.; Nian, Q.-G.; Song, Z.; Deng, Y.-Q.; Wang, X.; Zhu, S.-Y.; Li, X.-F.; Qin, C.-F.; *et al.* Hydrated Silica Exterior Produced by Biomimetic Silicification Confers Viral Vaccine Heat-Resistance. *ACS Nano* **2015**, *9*, 799–808.
- (36) Wang, G.; Cao, R.-Y.; Chen, R.; Mo, L.; Han, J.-F.; Wang, X.; Xu, X.; Jiang, T.; Deng,

- 1
2
3 Y.-Q.; Lyu, K.; *et al.* Rational Design of Thermostable Vaccines by Engineered Peptide-
4 Induced Virus Self-Biomineralization under Physiological Conditions. *Proc. Natl. Acad.*
5 *Sci.* **2013**, *110*, 7619–7624.
6
7
8
9
10
11 (37) Haase, N. R.; Shian, S.; Sandhage, K. H.; Kröger, N. Biocatalytic Nanoscale Coatings
12 through Biomimetic Layer-by-Layer Mineralization. *Adv. Funct. Mater.* **2011**, *21*, 4243–
13 4251.
14
15
16
17
18
19 (38) Begum, G.; Goodwin, W. B.; DeGlee, B. M.; Sandhage, K.; Kroeger, N.
20 Compartmentalisation of Enzymes for Cascade Reactions through Biomimetic Layer-by-
21 Layer Mineralization. *J. Mater. Chem. B* **2015**, *3*, 5232–5240.
22
23
24
25
26
27 (39) Sanchez-Sanchez, L.; Tapia-Moreno, A.; Juarez-Moreno, K.; Patterson, D.; Cadena-Nava,
28 R.; Douglas, T.; Vazquez-Duhalt, R. Design of a VLP-Nanovehicle for CYP450
29 Enzymatic Activity Delivery. *J. Nanobiotechnology* **2015**, *13*, 66.
30
31
32
33
34
35 (40) Qazi, S.; Miettinen, H. M.; Wilkinson, R. A.; McCoy, K.; Douglas, T.; Wiedenheft, B.
36 Programmed Self-Assembly of an Active P22-Cas9 Nanocarrier System. *Mol. Pharm.*
37 **2016**, *13*, 1191–1196.
38
39
40
41
42
43 (41) Anand, P.; O’Neil, A.; Lin, E.; Douglas, T.; Holford, M. Tailored Delivery of Analgesic
44 Ziconotide across a Blood Brain Barrier Model Using Viral Nanocontainers. *Sci. Rep.*
45 **2015**, *5*, Article No. 12497.
46
47
48
49
50
51 (42) Karimi, M.; Mirshekari, H.; Moosavi Basri, S. M.; Bahrami, S.; Moghoofei, M.; Hamblin,
52 M. R. Bacteriophages and Phage-Inspired Nanocarriers for Targeted Delivery of
53 Therapeutic Cargos. *Adv. Drug Deliv. Rev.* **2016**, *106*, 45–62.
54
55
56
57
58
59
60

- 1
2
3
4
5
6
7
8
9
10
11
12
13
14
15
16
17
18
19
20
21
22
23
24
25
26
27
28
29
30
31
32
33
34
35
36
37
38
39
40
41
42
43
44
45
46
47
48
49
50
51
52
53
54
55
56
57
58
59
60
- (43) Frietze, K. M.; Peabody, D. S.; Chackerian, B. Engineering Virus-like Particles as Vaccine Platforms. *Curr. Opin. Virol.* **2016**, *18*, 44–49.
- (44) Patterson, D. P.; Prevelige, P. E.; Douglas, T. Nanoreactors by Programmed Enzyme Encapsulation inside the Capsid of the Bacteriophage P22. *ACS Nano* **2012**, *6*, 5000–5009.
- (45) Patterson, D. P.; Schwarz, B.; Waters, R. S.; Gedeon, T.; Douglas, T. Encapsulation of an Enzyme Cascade within the Bacteriophage P22 Virus-like Particle. *ACS Chem. Biol.* **2014**, *9*, 359–365.
- (46) Ross, J. F.; Bridges, A.; Fletcher, J. M.; Shoemark, D.; Alibhai, D.; Bray, H. E. V; Beesley, J. L.; Dawson, W. M.; Hodgson, L. R.; Mantell, J.; *et al.* Decorating Self-Assembled Peptide Cages with Proteins. *ACS Nano* **2017**, *11*, 7901–7914.
- (47) Fletcher, J. M.; Boyle, A. L.; Bruning, M.; Bartlett, G. J.; Vincent, T. L.; Zaccai, N. R.; Armstrong, C. T.; Bromley, E. H. C.; Booth, P. J.; Brady, R. L.; *et al.* A Basis Set of de Novo Coiled-Coil Peptide Oligomers for Rational Protein Design and Synthetic Biology. *ACS Synth. Biol.* **2012**, *1*, 240–250.
- (48) Richardson, D. S. *Euler's Gem: The Polyhedron Formula and the Birth of Topology*; Preinceton Univeristy Press: Princeton, NJ, USA, 2008.
- (49) Kroto, H. W.; Heath, J. R.; O'Brien, S. C.; Curl, R. F.; Smalley, R. E. C60: Buckminsterfullerene. *Nature* **1985**, *318*, 162–163.
- (50) Mosayebi, M.; Shoemark, D. K.; Fletcher, J. M.; Sessions, R. B.; Linden, N.; Woolfson, D. N.; Liverpool, T. B. Beyond Icosahedral Symmetry in Packings of Proteins in

- 1
2
3 Spherical Shells. *Proc. Natl. Acad. Sci.* **2017**, *114*, 9014–9019.
4
5
6
7 (51) Wang, X.; Sun, C.; Li, P.; Wu, T.; Zhou, H.; Yang, D.; Liu, Y.; Ma, X.; Song, Z.; Nian,
8 Q.; *et al.* Vaccine Engineering with Dual-Functional Mineral Shell: A Promising Strategy
9 to Overcome Preexisting Immunity. *Adv. Mater.* **2016**, *28*, 694–700.
10
11
12
13
14 (52) Lear, S.; Cobb, S. L. Pep-Calc.com: A Set of Web Utilities for the Calculation of Peptide
15 and Peptoid Properties and Automatic Mass Spectral Peak Assignment. *J. Comput. Aided.*
16 *Mol. Des.* **2016**, *30*, 271–277.
17
18
19
20
21
22 (53) Baker, E. G.; Bartlett, G. J.; Crump, M. P.; Sessions, R. B.; Linden, N.; Faul, C. F. J.;
23 Woolfson, D. N. Local and Macroscopic Electrostatic Interactions in Single α -Helices.
24 *Nat. Chem. Biol.* **2015**, *11*, 221–228.
25
26
27
28
29
30 (54) Belton, D. J.; Deschaume, O.; Perry, C. C. An Overview of the Fundamentals of the
31 Chemistry of Silica with Relevance to Biosilicification and Technological Advances.
32 *FEBS J.* **2012**, *279*, 1710–1720.
33
34
35
36
37
38 (55) Nikolaychuk, P. A. The Revised Pourbaix Diagram for Silicon. *Silicon* **2014**, *6*, 109–116.
39
40
41 (56) Delalat, B.; Sheppard, V. C.; Rasi Ghaemi, S.; Rao, S.; Prestidge, C. A.; McPhee, G.;
42 Rogers, M.-L.; Donoghue, J. F.; Pillay, V.; Johns, T. G.; *et al.* Targeted Drug Delivery
43 Using Genetically Engineered Diatom Biosilica. *Nat. Commun.* **2015**, *6*, Article No. 8791.
44
45
46
47
48
49 (57) de Boer, P.; Hoogenboom, J. P.; Giepmans, B. N. G. Correlated Light and Electron
50 Microscopy: Ultrastructure Lights Up! *Nat. Methods* **2015**, *12*, 503–513.
51
52
53
54
55 (58) Müller-Reichert, T.; Verkade., P. *Correlative Light and Electron Microscopy*; Müller-
56 Reichert, T.; Verkade., P., Eds.; Oxford Academic Press: Oxford, UK, 2012.
57
58
59
60

- 1
2
3
4
5
6
7
8
9
10
11
12
13
14
15
16
17
18
19
20
21
22
23
24
25
26
27
28
29
30
31
32
33
34
35
36
37
38
39
40
41
42
43
44
45
46
47
48
49
50
51
52
53
54
55
56
57
58
59
60
- (59) Loike, J. D.; Silverstein, S. C. A Fluorescence Quenching Technique Using Trypan Blue to Differentiate between Attached and Ingested Glutaraldehyde-Fixed Red Blood Cells in Phagocytosing Murine Macrophages. *J. Immunol. Methods* **1983**, *57*, 373–379.
- (60) Sahlin, S.; Hed, J.; Runfquist, I. Differentiation between Attached and Ingested Immune Complexes by a Fluorescence Quenching Cytofluorometric Assay. *J. Immunol. Methods* **1983**, *60*, 115–124.
- (61) Mura, S.; Nicolas, J.; Couvreur, P. Stimuli-Responsive Nanocarriers for Drug Delivery. *Nat. Mater.* **2013**, *12*, 991–1003.
- (62) Rother, M.; Nussbaumer, M. G.; Renggli, K.; Bruns, N. Protein Cages and Synthetic Polymers: A Fruitful Symbiosis for Drug Delivery Applications, Bionanotechnology and Materials Science. *Chem. Soc. Rev.* **2016**, *45*, 6213–6249.
- (63) Zhang, X. F.; Mansouri, S.; Clime, L.; Ly, H. Q.; Yahia, L. 'H; Veres, T. Fe₃O₄-Silica Core-Shell Nanoporous Particles for High-Capacity pH-Triggered Drug Delivery. *J. Mater. Chem.* **2012**, *22*, 14450–14457.
- (64) Wang, X.; Schröder, H. C.; Müller, W. E. G. Enzyme-Based Biosilica and Biocalcite: Biomaterials for the Future in Regenerative Medicine. *Trends Biotechnol.* **2014**, *32*, 441–447.
- (65) Galloway, J. M.; Staniland, S. S. Protein and Peptide Biotemplated Metal and Metal Oxide Nanoparticles and Their Patterning onto Surfaces. *J. Mater. Chem.* **2012**, *22*, 12423–12434.
- (66) Galloway, J. M.; Bramble, J. P.; Staniland, S. S. Biomimetic Synthesis of Materials for

- 1
2
3 Technology. *Chem. – A Eur. J.* **2013**, *19*, 8710–8725.
4
5
6
7 (67) Oh, M. H.; Yu, J. H.; Kim, I.; Nam, Y. S. Genetically Programmed Clusters of Gold
8 Nanoparticles for Cancer Cell-Targeted Photothermal Therapy. *ACS Appl. Mater.*
9 *Interfaces* **2015**, *7*, 22578–22586.
10
11
12
13
14 (68) Górzny, M. Ł.; Walton, A. S.; Evans, S. D. Synthesis of High-Surface-Area Platinum
15 Nanotubes Using a Viral Template. *Adv. Funct. Mater.* **2010**, *20*, 1295–1300.
16
17
18
19
20 (69) Fields, G. B.; Noble, R. L. Solid Phase Peptide Synthesis Utilizing 9-
21 Fluorenylmethoxycarbonyl Amino Acids. *Int. J. Pept. Protein Res.* **1990**, *35*, 161–214.
22
23
24
25
26 (70) Ruiz-Gayo, M.; Albericio, F.; Pons, M.; Royo, M.; Pedroso, E.; Giralt, E. Uteroglobin-like
27 Peptide Cavities I. Synthesis of Antiparallel and Parallel Dimers of Bis-Cysteine Peptides.
28 *Tetrahedron Lett.* **1988**, *29*, 3845–3848.
29
30
31
32
33
34 (71) Schuck, P. Size-Distribution Analysis of Macromolecules by Sedimentation Velocity
35 Ultracentrifugation and Lamm Equation Modeling. *Biophys. J.* **2000**, *78*, 1606–1619.
36
37
38
39 (72) UTHSCSA. Ultrascan <http://ultrascan.uthscsa.edu/> (accessed Feb 22, 2017).
40
41
42
43 (73) Hurton, T.; Wright, A.; Deubler, G.; Bashir, B. SEDNTERP Daemon Version: 20120828
44 BETA <http://sednterp.unh.edu/> (accessed Feb 22, 2017).
45
46
47
48 (74) Alexander, G. B. The Preparation of Monosilicic Acid. *J. Am. Chem. Soc.* **1953**, *75*, 2887–
49 2888.
50
51
52
53
54 (75) Shimizu, K.; Del Amo, Y.; Brzezinski, M. A.; Stucky, G. D.; Morse, D. E. A Novel
55 Fluorescent Silica Tracer for Biological Silicification Studies. *Chem. Biol.* **2001**, *8*, 1051–
56
57
58
59
60

1
2
3 1060.
4
5

- 6
7 (76) Abramoff, M. D.; Magalhaes, P. J.; Ram, S. J. Image Processing with Image J.
8
9 *Biophotonics Int.* **2004**, *11*, 36–42.
10
11
12 (77) Schindelin, J.; Rueden, C. T.; Hiner, M. C.; Eliceiri, K. W. The ImageJ Ecosystem: An
13
14 Open Platform for Biomedical Image Analysis. *Mol. Reprod. Dev.* **2015**, *82*, 518–529.
15
16
17 (78) Kremer, J. R.; Mastronarde, D. N.; McIntosh, J. R. Computer Visualization of Three-
18
19 Dimensional Image Data Using IMOD. *J. Struct. Biol.* **1996**, *116*, 71–76.
20
21
22
23 (79) Mastronarde, D. N. Dual-Axis Tomography: An Approach with Alignment Methods That
24
25 Preserve Resolution. *J. Struct. Biol.* **1997**, *120*, 343–352.
26
27
28
29 (80) Schindelin, J.; Arganda-Carreras, I.; Frise, E.; Kaynig, V.; Longair, M.; Pietzsch, T.;
30
31 Preibisch, S.; Rueden, C.; Saalfeld, S.; Schmid, B.; *et al.* Fiji: An Open-Source Platform
32
33 for Biological-Image Analysis. *Nat. Methods* **2012**, *9*, 676–682.
34
35
36
37
38
39

40 Figure Legends

41
42 **Figure 1. Schematic for Self-Assembled peptide caGE (SAGE)¹ design and silicification.** A
43
44 homotrimerizing coiled-coil peptide (CC-Tri3, green) is joined back-to-back *via* a disulfide bond
45
46 to one of two heterodimeric sequences, namely a negatively charged CC-Di-A peptide (red) or a
47
48 positively charged CC-Di-B peptide (blue). These give hub A (CC-Tri3-CC-Di-A) and hub B
49
50 (CC-Tri3-CC-Di-B), respectively. When mixed, the hubs are posited to form a regular hexagonal
51
52 array that closes to form SAGEs. To ensure that silica precipitation is localized onto the SAGEs
53
54
55
56
57
58
59
60

1
2
3 when immersed in silicic acid, the *N* termini or *C* termini of the homotrimers are decorated with
4 positively charged peptides.
5
6

7
8
9
10 **Figure 2. Representative transmission electron microscopy (TEM) images of silicic acid**
11 **treated SAGE particles and controls.** (a, e, i) Cartoons showing peptide modules (left) and
12 assembled SAGEs (right). (b – d) Controls showing (b) silica precipitated in the absence of
13 peptide, (c) with parent SAGE, and (d) parent SAGE without silicic acid added. (f – h) Silicic-
14 acid treated SAGE with *N*-terminally appended tetrapeptides (f) E4-SAGE, (g) K4-SAGE and
15 (h) R4-SAGE. (j – l) as in panels f – h, but for *C*-terminally decorated SAGEs. Samples were
16 prepared at a concentration of 2 μ M peptide, 24 mM silicic acid, phosphate (PI) buffer (10 mM
17 potassium phosphate (8.02 mM dibasic K_2HPO_4 , 1.98 mM monobasic KH_2PO_4), pH 7.4),
18 24 hours, 20 °C. Scale bars are 200 nm.
19
20
21
22
23
24
25
26
27
28
29
30
31

32 **Figure 3. Summary of structures assembled during optimization of SiO_2 -R4-SAGE**
33 **formation.** (a) A fine network or mesh of disordered mineralized peptide, (b) spheres
34 interconnected with fine mesh, and (c) spheres interconnected with assembled mineralized
35 peptide. Individual SAGEs that are small (d), and regularly sized (e) (highlighted in yellow in
36 panel f) can also be produced. (f) Summary indicating how changing silicic acid and peptide
37 concentrations, proportion of parent SAGE, pH and temperature, alter the types of assemblies
38 observed for the SiO_2 -R4-SAGEs. The “Goldilocks zone” for making individual, regularly sized,
39 spherical SAGEs is highlighted in yellow. Arrows represent increasing values of the condition
40 illustrated.
41
42
43
44
45
46
47
48
49
50
51
52
53
54

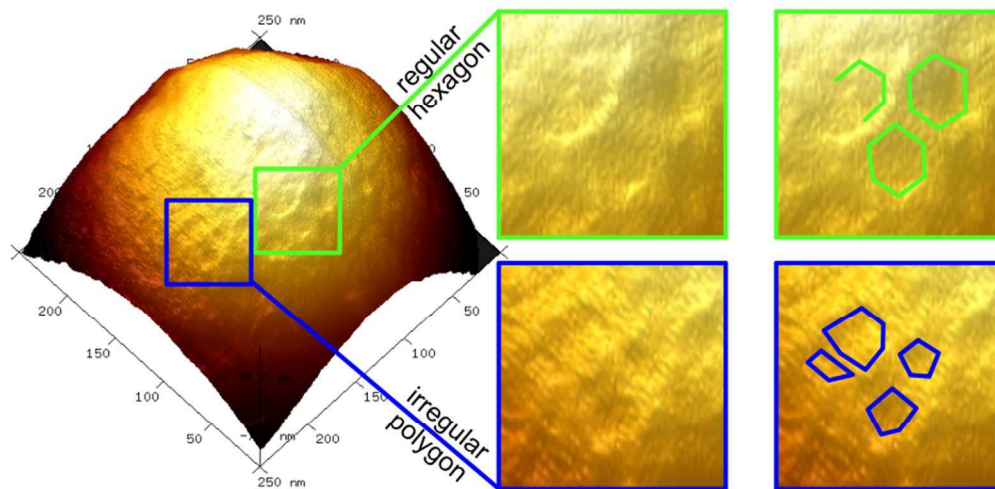
55 **Figure 4. PeakForce atomic force microscopy (PF-AFM) of SiO_2 -R4-SAGE particles on**
56 **mica.** 2D plots show variations recorded in (a) the height, (b) adhesion, and (c) dissipation
57
58
59
60

1
2
3 properties of the SiO₂-R4-SAGEs (upper parts of images) and mica (lower parts of images). (d)
4
5 A 3D plot of the topography. The mica surface is smooth, whereas the SiO₂-R4-SAGE surface
6
7 reveals texture, which is shown in greater detail in Figure 5. Silicification was performed with
8
9 2 μM peptide, 12 mM silicic acid, PI buffer, 24 hours, 20 °C.
10
11
12
13

14 **Figure 5. PeakForce atomic force microscopy (PF-AFM) of an individual SiO₂-R4-SAGE**
15 **particle.** 2D plots zoomed in on area shown in Figure 4, which map variation in (a) height, (b)
16
17 adhesion, and (c) dissipation, and a plot showing (d) height contrast. (e) The same surface as
18
19 shown in (d) with the corresponding adhesion map overlaid as a blue-scale color-map, which
20
21 shows that variations in topography and adhesion co-localize. (f – i) 3x magnifications for (f &
22
23 g) 3D height plots and (h & i) height-adhesion overlays, revealing (f & h) irregular polygons and
24
25 (g & i) regular hexagons. (j – m) Annotated version of panels f – i with shapes drawn to guide
26
27 the eye. Silicification was performed with 2 μM peptide, 12 mM silicic acid, PI buffer, 24 hours,
28
29 20 °C.
30
31
32
33
34
35
36

37 **Figure 6. Correlative light and electron microscopy (CLEM) and fluorescence microscope**
38 **images of R4-SAGE-fl fluorescent SAGEs.** (a) Schematic showing the peptide modules used to
39
40 assemble R4-SAGE-fls (2 μM peptide, PI buffer, 1 hour, 20 °C). (b) High-magnification TEM
41
42 image of a cluster of SiO₂-R4-SAGE-fls (mineralization conditions: 24 mM silicic acid,
43
44 24 hours, PI buffer, 20 °C). (c & d) TEM images superimposed with fluorescence microscope
45
46 images of the same area to produce CLEM images. In c & d, red boxes highlight the zoomed
47
48 area for the previous panel. (e – p) Fluorescence microscope images of R4-SAGE-fls (scale bars
49
50 10 μm): (e – h) unmineralized; mineralized with (i – l) 12 mM silicic acid; and (m – p) 24 mM
51
52 silicic acid. Separate bright-field and overlaid images are given in Figure S26. R4-SAGE-fls
53
54
55
56
57
58
59
60

1
2
3 without additives (e, i, m), and after treatment with: (f, j, n) Trypan blue; (g, k, n) tris(2-
4 carboxyethyl)phosphine hydrochloride (TCEP); and (h, l, p) trypsin.
5
6
7
8
9
10
11
12
13
14
15
16
17
18
19
20
21
22
23
24
25
26
27
28
29
30
31
32
33
34
35
36
37
38
39
40
41
42
43
44
45
46
47
48
49
50
51
52
53
54
55
56
57
58
59
60



TOC entry

79x42mm (300 x 300 DPI)

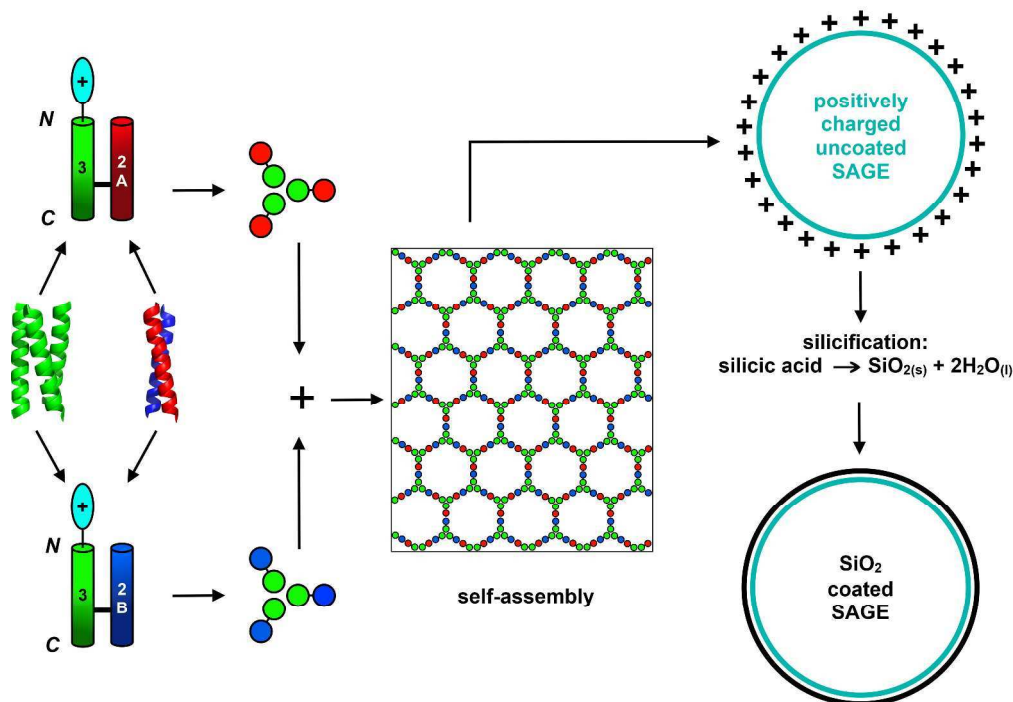


Figure 1. Schematic for Self-Assembled peptide caGE (SAGE)¹ design and silicification. A homotrimerizing coiled-coil peptide (CC-Tri3, green) is joined back-to-back *via* a disulfide bond to one of two heterodimeric sequences, namely a negatively charged CC-Di-A peptide (red) or a positively charged CC-Di-B peptide (blue). These give hub A (CC-Tri3-CC-Di-A) and hub B (CC-Tri3-CC-Di-B), respectively. When mixed, the hubs are positioned to form a regular hexagonal array that closes to form SAGEs. To ensure that silica precipitation is localized onto the SAGEs when immersed in silicic acid, the *N* termini or *C* termini of the homotrimers are decorated with positively charged peptides.

344x242mm (300 x 300 DPI)

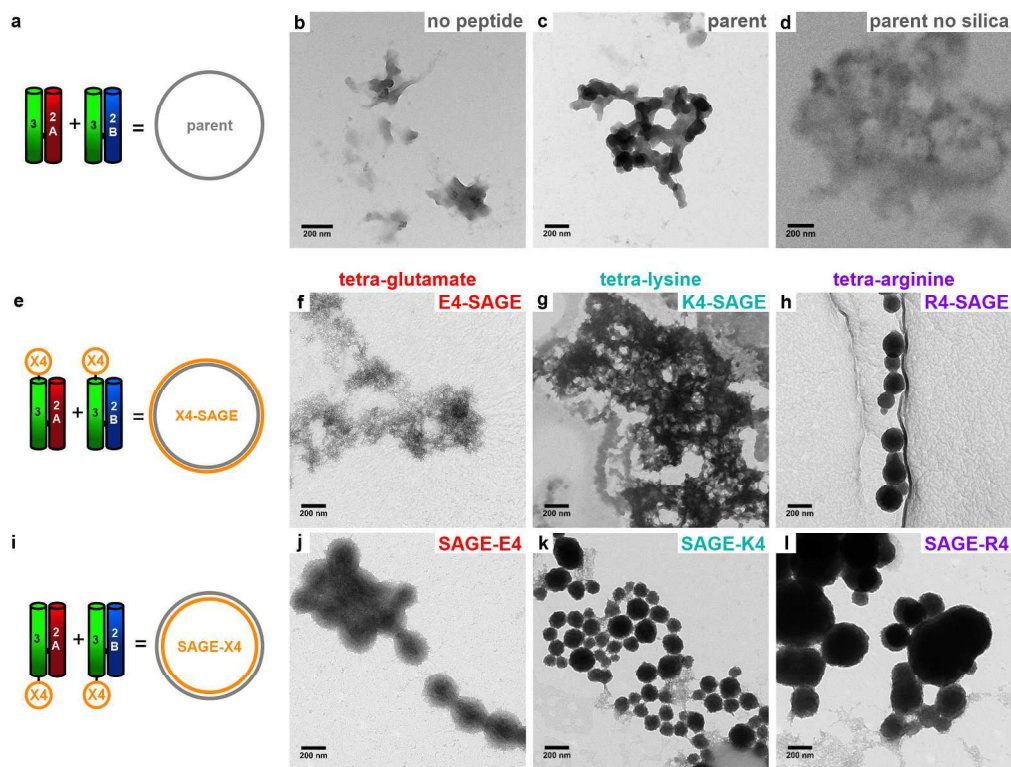


Figure 2. Representative transmission electron microscopy (TEM) images of silicic acid treated SAGE particles and controls. (a, e, i) Cartoons showing peptide modules (left) and assembled SAGEs (right). (b – d) Controls showing (b) silica precipitated in the absence of peptide, (c) with parent SAGE, and (d) parent SAGE without silicic acid added. (f – h) Silicic-acid treated SAGE with *N*-terminally appended tetrapeptides (f) E4-SAGE, (g) K4-SAGE and (h) R4-SAGE. (j – l) as in panels f – h, but for *C*-terminally decorated SAGEs. Samples were prepared at a concentration of 2 μ M peptide, 24 mM silicic acid, phosphate (PI) buffer (10 mM potassium phosphate (8.02 mM dibasic K_2HPO_4 , 1.98 mM monobasic KH_2PO_4), pH 7.4), 24 hours, 20 $^{\circ}C$. Scale bars are 200 nm.

296x224mm (200 x 200 DPI)

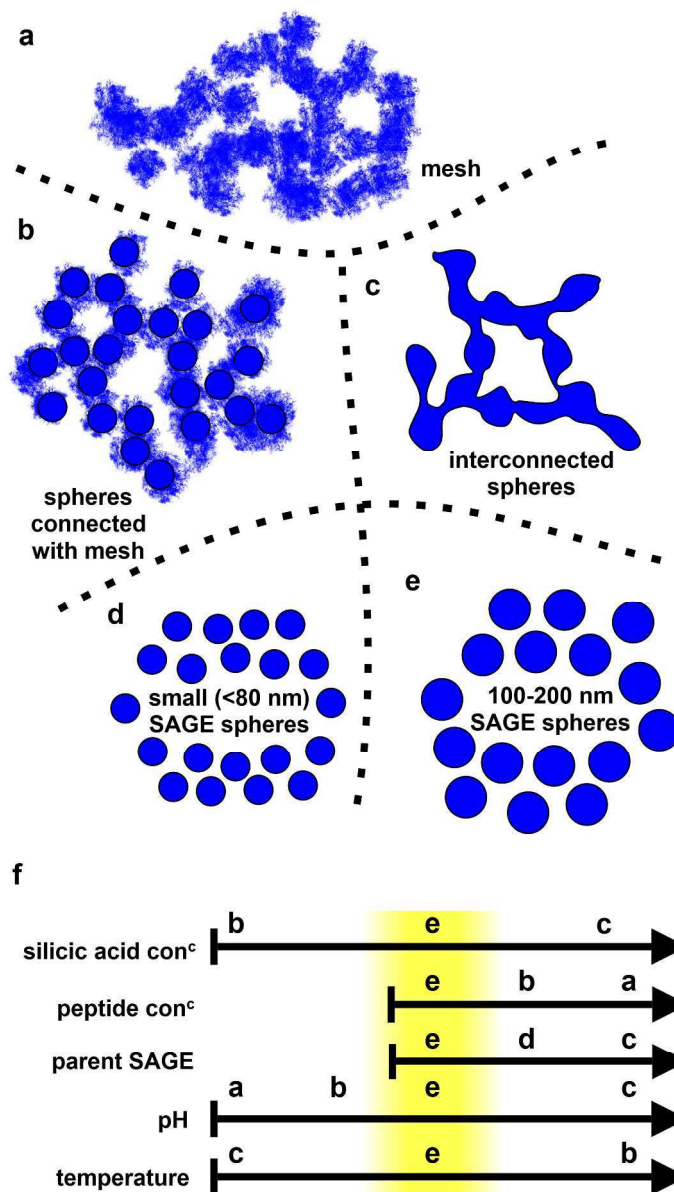


Figure 3. Summary diagram of the structures assembled during optimization of SiO₂-R4-SAGE formation. (a) A fine network or mesh of disordered mineralized peptide, (b) spheres interconnected with fine mesh, and (c) spheres interconnected with assembled mineralized peptide. Individual SAGEs that are (d) small, and (e) regularly sized (highlighted in yellow) can also be produced. (f) Shows how altering the: silicic acid, and peptide concentrations; proportion of parent SAGE; pH and temperature; alters the types of assemblies observed for the SiO₂-R4-SAGEs. The "Goldilocks" zone (just right for making individual, regularly sized, spherical SAGEs) is highlighted in yellow. Arrows represent increasing values of the condition illustrated.

168x292mm (300 x 300 DPI)

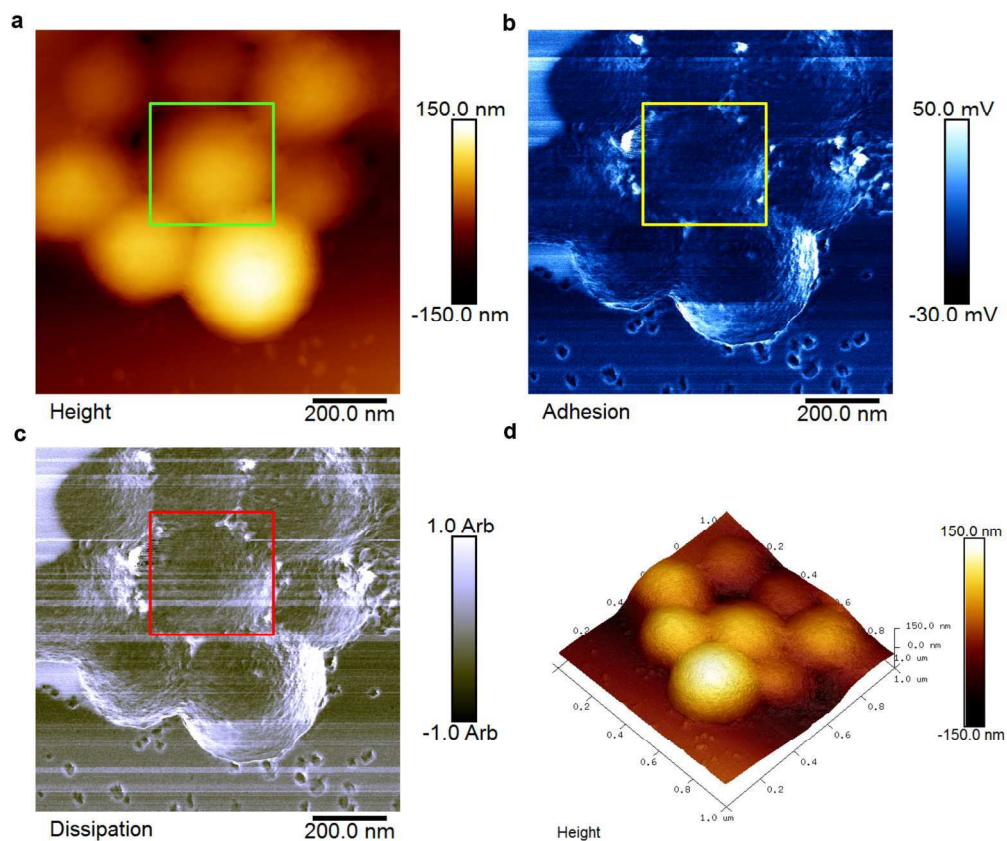


Figure 4. PeakForce atomic force microscopy (PF-AFM) of SiO₂-R4-SAGE particles on mica. 2D plots show variations recorded in (a) the height, (b) adhesion, and (c) dissipation properties of the SiO₂-R4-SAGES (upper parts of images) and mica (lower parts of images). (d) A 3D plot of the topography. The mica surface is smooth, whereas the SiO₂-R4-SAGE surface reveals texture, which is shown in greater detail in Figure 5. Silicification was performed with 2 μ M peptide, 12 mM silicic acid, PI buffer, 24 hours, 20 $^{\circ}$ C.

243x204mm (200 x 200 DPI)

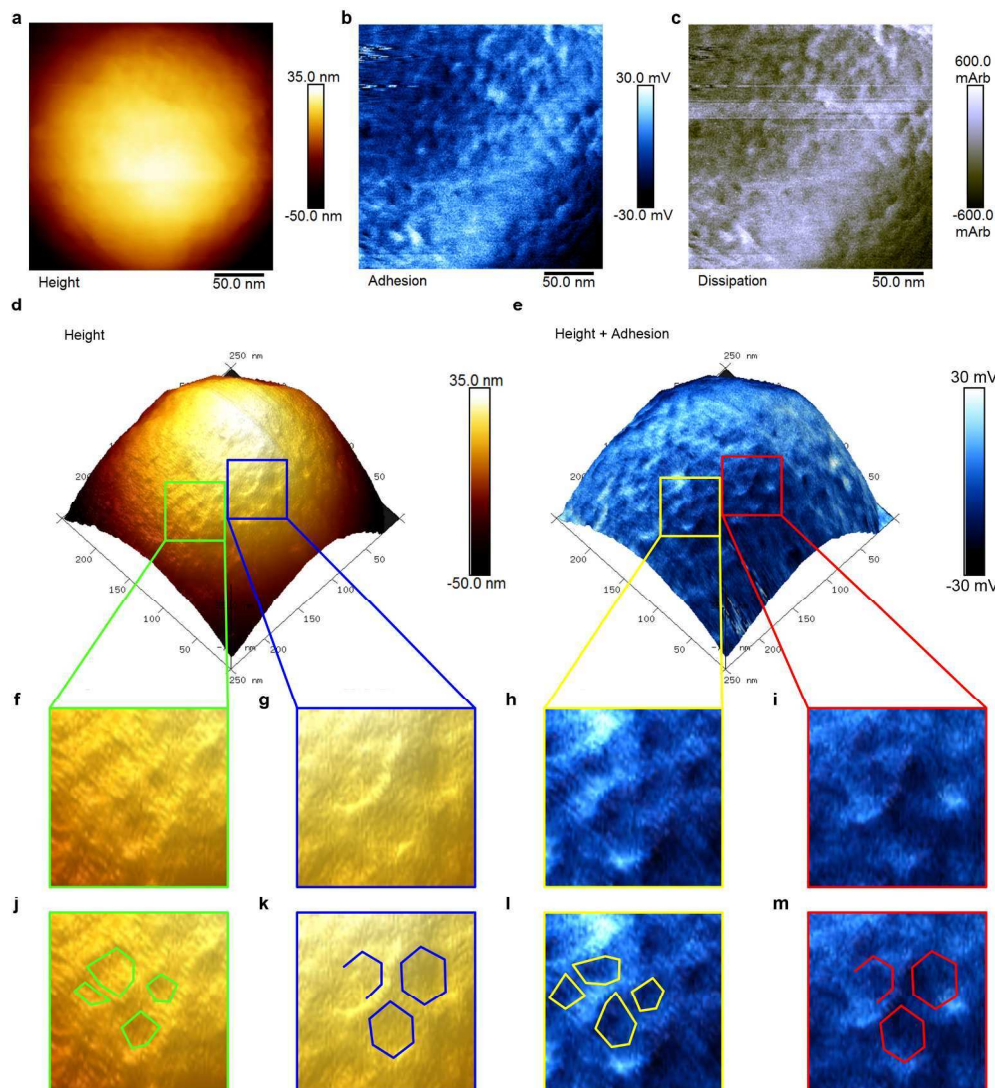


Figure 5. PeakForce atomic force microscopy (PF-AFM) of an individual SiO₂-R4-SAGE particle. 2D plots zoomed in on area shown in Figure 4, which map variation in (a) height, (b) adhesion, and (c) dissipation, and a plot showing (d) height contrast. (e) The same surface as shown in (d) with the corresponding adhesion map overlaid as a blue-scale color-map, which shows that variations in topography and adhesion co-localize. (f – i) 3x magnifications for (f & g) 3D height plots and (h & i) height-adhesion overlays, revealing (f & h) irregular polygons and (g & i) regular hexagons. (j – m) Annotated version of panels f – i with shapes drawn to guide the eye. Silicification was performed with 2 μ M peptide, 12 mM silicic acid, PI buffer, 24 hours, 20 $^{\circ}$ C.

303x329mm (200 x 200 DPI)

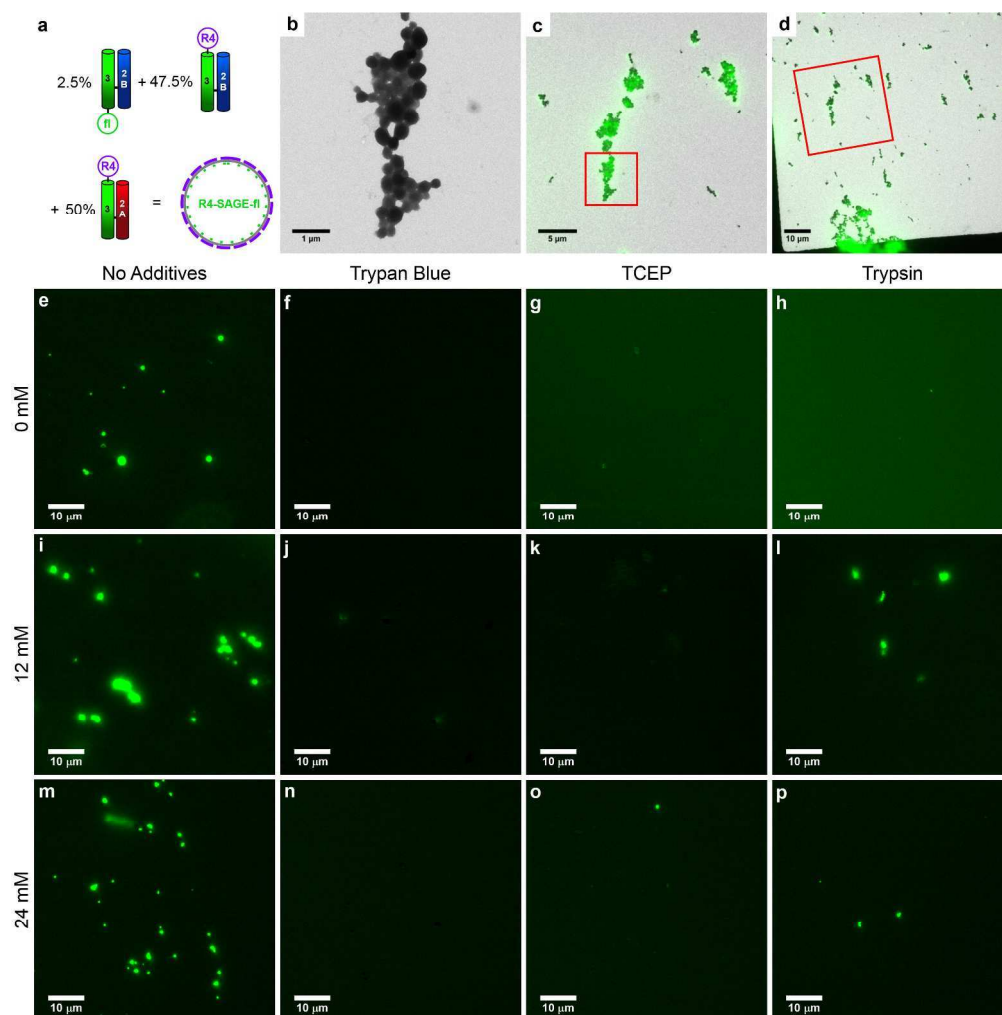


Figure 6. Correlative light and electron microscopy (CLEM) and fluorescence microscope images of R4-SAGE-fl fluorescent SAGEs. (a) Schematic showing the peptide modules used to assemble R4-SAGE-fls (2 μ M peptide, PI buffer, 1 hour, 20 $^{\circ}$ C). (b) High-magnification TEM image of a cluster of SiO₂-R4-SAGE-fls (mineralization conditions: 24 mM silicic acid, 24 hours, PI buffer, 20 $^{\circ}$ C). (c & d) TEM images superimposed with fluorescence microscope images of the same area to produce CLEM images. In c & d, red boxes highlight the zoomed area for the previous panel. (e - p) Fluorescence microscope images of R4-SAGE-fls (scale bars 10 μ m): (e - h) unmineralized; mineralized with (i - l) 12 mM silicic acid; and (m - p) 24 mM silicic acid. Separate bright-field and overlaid images are given in Figure S26. R4-SAGE-fls without additives (e, i, m), and after treatment with: (f, j, n) Trypan blue; (g, k, o) tris(2-carboxyethyl)phosphine hydrochloride (TCEP); and (h, l, p) trypsin.

374x377mm (200 x 200 DPI)